Inorg. Chem. **2005**, *44*, 1852–1866

Polymorphism in Fe[(*p*-IC$_6$H$_4$)B(3-Mepz)$_3$]$_2$ (pz = Pyrazolyl): Impact of Supramolecular Structure on an Iron(II) Electronic Spin-State Crossover

Daniel L. Reger,*,† James R. Gardinier,† Mark D. Smith,† Ahmed M. Shahin,‡ Gary J. Long,*,‡ Leila Rebbouh,§ and Fernande Grandjean§

Department of Chemistry and Biochemistry, University of South Carolina, Columbia, South Carolina 29208, Department of Chemistry, University of Missouri—Rolla, Rolla, Missouri 65409-0010, and Department of Physics, B5, University of Liège, B-4000 Sart-Tilman, Belgium

Received November 12, 2004

The new ligands Na[(*p*-IC$_6$H$_4$)B(3-Rpz)$_3$] (R = H, Me) have been prepared by converting I$_2$C$_6$H$_4$ to IC$_6$H$_4$SiMe$_3$ with Li^{t}Bu and SiMe$_3$Cl, and then to IC$_6$H$_4$BBr$_2$ with BBr$_3$ and subsequent reaction with 3 equiv of (un)substituted pyrazole and 1 equiv of NaO^{t}Bu. These new ligands react with FeBr$_2$ to give either purple, low-spin Fe[(*p*-IC$_6$H$_4$)B(pz)$_3$]$_2$ or colorless, high-spin Fe[(*p*-IC$_6$H$_4$)B(3-Mepz)$_3$]$_2$. Depending upon the crystallization conditions, Fe[(*p*-IC$_6$H$_4$)B(3-Mepz)$_3$]$_2$ can exist both as two polymorphs and as a methylene chloride solvate. An examination of these polymorphs by variable-temperature X-ray crystallography, magnetic susceptibility, and Mössbauer spectroscopy has revealed different electronic spin-state crossover properties for each polymorph and yields insight into the influence of crystal packing, independent of other electronic perturbations, on the spin-state crossover. The first polymorph of Fe[(*p*-IC$_6$H$_4$)B(3-Mepz)$_3$]$_2$ has a highly organized three-dimensional supramolecular structure and does not undergo a spin-state crossover upon cooling to 4 K. The second polymorph of Fe[(*p*-IC$_6$H$_4$)B(3-Mepz)$_3$]$_2$ has a stacked two-dimensional supramolecular structure, a structure that is clearly less well organized than that of the first polymorph, and undergoes an abrupt iron(II) spin-state crossover from high spin to low spin upon cooling below ca. 130 K. The crystal structure of the methylene chloride solvate of Fe[(*p*-IC$_6$H$_4$)B(3-Mepz)$_3$]$_2$ has a similar stacked two-dimensional supramolecular structure, but the crystals readily lose the solvate. The resulting desolvate undergoes a gradual spin-state crossover to the low-spin state upon cooling below ca. 235 K. It is clear from a comparison of the structures that the long-range solid-state organization of the molecules, which is controlled by noncovalent supramolecular interactions, has a strong impact upon the spin-state crossover, with the more highly organized structures having lower spin-crossover temperatures and more abrupt spin-crossover behavior.

Introduction

Octahedral iron(II) complexes that undergo a thermal spin-state crossover[1] have emerged from the realm of laboratory curiosities to the precipice of applied chemistry with such diverse applications as "intelligent" contrast agents for biomedical imaging,[2] temperature threshold indicators,[3] and optical elements in display devices.[3] The temperature dependence of the transition between the highly colored low-spin (LS) $^1A_{1g}$ ($t_{2g}^6e_g^{*0}$) state and the typically colorless or lightly colored high-spin (HS) $^5T_{2g}$ ($t_{2g}^4e_g^{*2}$) state of octahedral 3d^6 iron(II) complexes is exploited in the development of such devices. Generally, the temperature dependence of the spin transition shows any one of five behaviors—gradual, abrupt, stepwise, incomplete, or one with hysteresis—and each type of behavior dictates the ultimate application, if any, of the material. In this sense, there has been a

* To whom correspondence should be addressed. E-mail: reger@mail.chem.sc.edu (D.L.R.); glong@umr.edu (G.J.L.).
† University of South Carolina.
‡ University of Missouri—Rolla.
§ University of Liège.

(1) (a) Real, J. A.; Gaspar, A. B.; Niel, V.; Muñoz, M. C. *Coord. Chem. Rev.* **2003**, *236*, 121. (b) Gütlich, P.; Garcia, Y.; Goodwin, H. A. *Chem. Soc. Rev.* **2000**, *29*, 419. (c) Gütlich, P.; Hauser, A.; Spiering, H. *Angew. Chem., Int. Ed. Engl.* **1994**, *33*, 2024. (d) König, E.; Ritter, G.; Kulshreshtha, S. K. *Chem. Rev.* **1985**, *85*, 219. (e) Long, G. J.; Grandjean, F.; Reger, D. L. *Top. Curr. Chem.* **2004**, *233*, 91.

(2) Muller, R. N.; Vander Elst, L.; Laurent, S. *J. Am. Chem. Soc.* **2003**, *125*, 8405.

(3) Kahn, O.; Martinez, C. J. *Science* **1998**, *279*, 44.

10.1021/ic048406q CCC: $30.25
Published on Web 02/23/2005

considerable emphasis toward developing new examples of spin-transition materials in order to more fully understand the nature of the temperature dependence of the spin transitions. Complexes that contain the FeN_6 coordination environment are, by far, the most studied class of spin-transition complexes. Thus, reports of the spin-state crossover behavior of iron(II) derivatives of triazoles,[4] tetrazoles,[5] isoxazoles,[6] polypyridyls,[7] picolylamines,[8] cyanopyridines,[9] poly(pyrazolyl)borates,[10] and some pyrazolyl/pyridyl mixed ligand systems[11] are available. Our group has recently reported the unusual spin-state crossover behavior exhibited by both homoleptic and heteroleptic tris(pyrazolyl)methane iron(II) complexes.[12] In these complexes, the temperature dependence of the magnetic susceptibility was shown to be dependent on the nature of the counteranion, the included solvent, and the groups bound to the pyrazolyl rings. These results are consistent with other systems in that steric interactions involving groups proximal to the metal center favor the HS ground state and tend to decrease the temperature at which the resulting complexes undergo the spin-state crossover, and in some cases, the LS state may not even be accessible.

Several different and acceptable models have been put forth from a physical chemistry perspective, to describe the nature of spin-state transition behavior of various complexes.[1] These models, which incorporate terms such as "chemical pressure", "elastic interactions", and "lattice forces", account for the nature of the cooperativity in polymeric species connected by covalent bonding interactions (that give rise to abrupt rather than gradual spin transitions). However, the true meaning of these terms and, hence, the nature of the transitions in discrete molecular species or "isolated" cationic iron(II) species really becomes apparent only on the rare occurrence that two polymorphs of the same spin-transition compound can be found and examined in detail. To the best of our knowledge, the occurrence, identification, and characterization of iron(II) spin-crossover polymorphs has been limited to the heavily studied tetraaza complexes of $Fe(NCS)_2$.[13a−h] Of these, the recently described Fe(*N*-2-pyridylmethylene-4-aminobiphenyl)$_2$(NCS)$_2$ system,[13c] which crystallizes as two polymorphs (I and II), provides a nice example of how small and seemingly unimportant structural changes can lead to different magnetic behavior. Form I undergoes an abrupt HS-to-LS transition at 170 K, while the second (form II) undergoes a gradual transition centered around 205 K. The main difference in the two structures is that form I has a slightly more distorted FeN_6 octahedron and shorter, weak, intermolecular S···HC hydrogen-bonding interactions (between the sulfur of one NCS group on one iron molecule with a phenyl ring hydrogen from a neighboring molecule) compared to form II. Other related systems show even more diverse behavior. For instance, only one of the two polymorphs of Fe(2,2′-di-2-thiazoline)$_2$(NCS)$_2$ shows a HS−LS transition centered at 175 K (with hysteresis), while the second form remains HS at all temperatures.[13g] Also, Fe[(3-aminopropyl)bis(2-pyridylmethyl)amine](NCS)$_2$ exists as three polymorphs that show either an abrupt transition with hysteresis ($T_c\downarrow$ 112 K, $T_c\uparrow$ 120 K), a gradual transition without hysteresis (T_c 176 K), or no transition (HS only), depending on the extent of intermolecular π-stacking of pyridine rings and deformation of the FeN_6 octahedral coordination spheres.[13d] The possibility of using noncovalent interactions to control magnetic properties of molecular spin-crossover compounds is alluring from a supramolecular synthetic chemist's viewpoint and has seen some promise

(4) (a) Roubeau, O.; Gomez, J. M. A.; Balskus, E.; Kolnaar, J. J. A.; Haasnoot, J. G.; Reedjik, J. *New J. Chem.* **2001**, *25*, 144. (b) Kolnaar, J. J. A.; De Heer, M. I.; Kooijman, H.; Spek, A. L.; Schmitt, G.; Ksenofontov, V.; Gütlich, P.; Haasnoot, J. G.; Reedijk, J. *Eur. J. Inorg. Chem.* **1999**, *5*, 881. (c) Garcia, Y.; van Koningsbruggen, P. J.; Codjovi, E.; Lapouyade, R.; Kahn, O.; Rabardel, L. *J. Mater. Chem.* **1997**, *7*, 857.

(5) (a) Grunert, C. M.; Schweifer, J.; Weinberger, P. W.; Linert, W.; Mereiter, K.; Hilscher, G.; Muller, M.; Wiesinger, G.; van Koningsbruggen, P. J. *Inorg. Chem.* **2004**, *43*, 155. (b) Stassen, A. F.; Roubeau, O.; Ferrero Gramage, I.; Linares, J.; Varret, F.; Mutikainen, I.; Turpeinen, U.; Haasnoot, J. G.; Reedijk, J. *Polyhedron* **2001**, *20*, 1699.

(6) Hibbs, W.; van Koningsbruggen, P. J.; Arif, A. M.; Shum, W. W.; Miller, J. S. *Inorg. Chem.* **2003**, *42*, 5645.

(7) (a) Moliner, N.; Muñoz, M. C.; Letard, S.; Salmon, L.; Tuchagues, J.-P.; Bousseksou, A.; Real, J. A. *Inorg. Chem.* **2002**, *41*, 6997. (b) Moliner, N.; Salmon, L.; Capes, L.; Muñoz, M. C.; Tuchagues, J.-P.; Bousseksou, A.; McGarvey, J. J.; Dennis, A. C.; Castro, M.; Burriel, R.; Real, J. A. *J. Phys. Chem. B* **2002**, *106*, 4276. (c) Real, J. A.; Muñoz, M. C.; Faus, J.; Solans, X. *Inorg. Chem.* **1997**, *36*, 3008. (d) Müller, E. W.; Spiering, H.; Gütlich, P. *Chem. Phys. Lett.* **1982**, *93*, 567. (e) König, E.; Madeja, K.; Watson, K. J. *J. Am. Chem. Soc.* **1968**, *90*, 1146.

(8) Spiering, H.; Meissner, E.; Köppen, H.; Müller, E. W.; Gütlich, P. *Chem. Phys.* **1982**, *68*, 65.

(9) Galet, A.; Niel, V.; Muñoz, M. C.; Real, J. A. *J. Am. Chem. Soc.* **2003**, *125*, 14227.

(10) (a) Oliver, J. D.; Mullica, D. F.; Hutchinson, B. B.; Milligan, W. O. *Inorg. Chem.* **1980**, *19*, 195. (b) Jesson, J. P.; Trofimenko, S.; Eaton, D. R. *J. Am. Chem. Soc.* **1967**, *89*, 3158. (c) Jesson, J. P.; Weiher, J. F. *J. Chem. Phys.* **1967**, *46*, 1995. (d) Jesson, J. P.; Weiher, J. F.; Trofimenko, S. *J. Chem. Phys.* **1968**, *48*, 2058.

(11) (a) Leita, B. A.; Moubaraki, B.; Murray, K. S.; Smith, J. P.; Cashion, J. D. *Chem. Commun.* **2004**, 156. (b) Sugiyarto, K. H.; McHale, W.-A.; Craig, D. C.; Rae, A. D.; Scudder, M. L.; Goodwin, H. A. *Dalton Trans.* **2003**, 2443. (c) Manikandan, P.; Padmakumar, K.; Thomas, K. R. J.; Varghse, B.; Onodera, H.; Manoharan, P. T. *Inorg. Chem.* **2001**, *40*, 6930. (d) Holland, J. M.; Mcallister, J. A.; Lu, Z.; Kilner, C. A.; Thornton-Pett, M.; Halcrow, M. A. *Chem. Commun.* **2001**, 577. (e) Suemara, N.; Ohama, M.; Kaizaki, S. *Chem. Comm.* **2001**, 1538.

(12) (a) Piquer, C.; Grandjean, F.; Mathon, O.; Pascarelli, S.; Reger, D. L.; Little, C. A.; Long, G. J. *Inorg. Chem.* **2003**, *42*, 982. (b) Reger, D. L.; Little, C. A.; Smith, M. D.; Long, G. J. *Inorg. Chem.* **2002**, *41*, 4453. (c) Reger, D. L.; Little, C. A.; Smith, M. D.; Rheingold, A. L.; Lam, K.-C.; Concolina, T. L.; Long, G. J.; Hermann, R. P.; Grandjean, F. *Inorg. Chem.* **2002**, *41*, 1190. (d) Reger, D. L.; Wright, T. L.; Little, C. A.; Lamba, J. J. S.; Smith, M. D. *Inorg. Chem.* **2001**, *40*, 3810. (e) Reger, D. L.; Little, C. A.; Rheingold, A. L.; Sommer, R.; Long, G. J. *Inorg. Chim. Acta* **2001**, *40*, 1508. (f) Reger, D. L.; Little, C. A.; Rheingold, A. L.; Lam, M.; Liable-Sands, L. M.; Rhagitan, B.; Concolino, T.; Mohan, A.; Long, G. J.; Briois, V.; Grandjean, F. *Inorg. Chem.* **2001**, *40*, 1508. (g) Reger, D. L.; Wright, T. D.; Little, C. A.; Lamba, J. J. S.; Smith, M. D. *Inorg. Chem.* **2001**, *40*, 3810.

(13) (a) Ksenofontov, V.; Gaspar, A. B.; Levchenko, G.; Fitzsimmons, B.; Gütlich, P. *J. Phys. Chem. B* **2004**, *108*, 7723. (b) Thompson, A. L.; Goeta, A. E.; Real, J. A.; Galet, A.; Muñoz, M. C. *Chem. Commun* **2004**, 1390. (c) Marchivie, M.; Guionneau, P.; Létard, J.-F.; Chasseau, D. *Acta Crystallogr.* **2003**, *B59*, 479. (d) Matouzenko, G. S.; Bousseksou, A.; Lecocq, S.; van Koningsbruggen, P. J.; Perrin, M.; Kahn, O.; Collet, A. *Inorg. Chem.* **1997**, *36*, 5869. (e) Sugiyarto, K. H.; Craig, D. C.; Goodwin, H. A. *Aust. J. Chem.* **1996**, *49*, 497. (f) Konno, M.; Mikami-Kido, M. *Bull. Chem. Soc. Jpn.* **1991**, *64*, 339. (g) Ozarowski, A.; McGarvey, B. R.; Sarkar, A. B.; Drake, J. E. *Inorg. Chem.* **1988**, *27*, 628. (h) König, E.; Madeja, K.; Watson, K. J. *J. Am. Chem. Soc.* **1968**, *90*, 1146. (i) König, E.; Madeja, K. *Inorg. Chem.* **1967**, *6*, 48. (j) Guionneau, P.; Létard, J.-F.; Yufit, D. S.; Chasseau, D.; Bravic, G.; Goeta, A. E.; Howard, J. A. K.; Kahn, O. *J. Mater. Chem.* **1999**, *9*, 985.

from the studies of arylazoanilinedi(isothiocyanato)iron(II) complexes.[13j]

During the course of a recent comprehensive systematic study that we have undertaken to design systems that promote specific covalent and noncovalent interactions with the goal of determining how these forces impact the spin-state transitions in both tris(pyrazolyl)methane and tris(pyrazolyl)-borate iron(II) complexes, we have discovered that the magnetic properties of $Fe[(p\text{-}IC_6H_4)B(3\text{-}Mepz)_3]_2$ exhibited an unusual sample dependence. Some samples exhibited spin-state transitions, as first indicated by a change in color on cycling the temperature of the sample between 294 and 78 K, whereas other samples did not. In this contribution, we outline the differences in the ground-state magnetic properties of the $Fe[(p\text{-}IC_6H_4)B(3\text{-}Rpz)_3]_2$ (R = H, Me) complexes. By studying the unusual sample-dependent magnetic, structural, and Mössbauer behavior observed with two polymorphs and a methylene chloride solvate form of the 3-methylpyrazolyl derivative, we have been able to correlate the supramolecular structure of discrete molecular poly(pyrazolyl)borate iron-(II) complexes with the temperature dependence of their spin-state crossover behavior. This foundation will be expanded upon in future papers with the goal of more precisely defining both the intramolecular and intermolecular forces that are responsible for the cooperative interactions and whether the cooperative interactions lead to or fail to lead to an electronic spin-state crossover.

Experimental Section

General Considerations. All operations were carried out either under a nitrogen atmosphere using standard Schlenk techniques or in a Vacuum Atmospheres HE-493 inert atmosphere drybox, unless otherwise specified. Solvents for synthetic procedures and spectroscopic studies were dried by conventional methods and distilled under a N_2 atmosphere immediately prior to use. BBr_3 was used as received from Strem Chemicals. All other chemicals were purchased from Aldrich Chemicals. Pyrazole was sublimed and 3-methylpyrazole was distilled under vacuum before use. Robertson Microlit Laboratories performed all elemental analyses. Melting point determinations were made on samples contained in glass capillaries by using an Electrothermal 9100 apparatus and are uncorrected. Mass spectrometric measurements recorded in ESI(±) mode were obtained on a Micromass Q-Tof spectrometer, whereas those performed by direct probe analyses were made on a VG 70S instrument. NMR spectra were recorded by using either a Varian Gemini 300 or a Varian Mercury 400 instrument, as noted within the text. Chemical shifts were referenced to solvent resonances at δ_H 2.05 and δ_C 29.8 for acetone-d_6, δ_H 7.27 and δ_C 77.23 for $CDCl_3$, and δ_H 3.31 and δ_C 49.15 for CD_3OD.

Magnetic susceptibilities were measured at 0.5 T using a Quantum Design MPMS XL SQUID magnetometer. Gelatin capsules were used as sample containers for measurements taken in the temperature range 5−300 K. The very small diamagnetic contribution of the gelatin capsule had a negligible contribution to the overall magnetization, which was dominated by the sample. The molar magnetic susceptibilities were corrected for the diamagnetism of the complexes, which was calculated from tables of Pascal's constants to be -454×10^{-6} emu/mol for $Fe[(p\text{-}IC_6H_4)B(3\text{-}Mepz)_3]_2$.

The Mössbauer spectral absorber contained ca. 50 mg/cm^2 of powder mixed with boron nitride, and the spectra were measured between 4.2 and 295 K on a constant-acceleration spectrometer that utilized a room-temperature rhodium matrix cobalt-57 source and was calibrated at room temperature with α-iron foil. The estimated absolute errors are ±0.005 mm/s for the isomer shifts, ±0.01 mm/s for the quadrupole splittings and line widths, and ±0.2% for the relative spectral absorption areas.

Syntheses. $p\text{-}IC_6H_4SiMe_3$. This complex was prepared by a modification of the literature procedure.[14] An 88.6 mL (151.5 mmol) portion of Li(^{t}Bu) as a 1.7 M solution in pentane was added dropwise over the period of 20 min to a cold suspension (−78 °C) of 25.0 g (75.8 mmol) of $p\text{-}I_2C_6H_4$. A yellow solution formed after one-half of the Li(^{t}Bu) was added, and after complete addition the resulting yellow suspension was stirred for 1.5 h at −78 °C. A 15 mL (118.2 mmol) aliquot of $SiMe_3Cl$ was added by syringe to the cold suspension, and the mixture was stirred for an additional hour. The mixture was then stirred to room temperature for 1 h and was poured into 100 mL of a 4% $NaHCO_3$ solution. The organic and aqueous layers were separated, and the aqueous layer was extracted twice with 100 mL of Et_2O. The combined organics were dried over $MgSO_4$, solvent was removed by rotary evaporation, and the residual yellow oil was passed through a silica gel plug (eluting with hexanes) to remove colored impurities (alternatively, the crude yellow oil could be distilled under vacuum at 83−85 °C/1 mmHg). The solvent was removed by rotary evaporation to leave 20.23 g (97%, if pure) of crude $p\text{-}IC_6H_4SiMe_3$ as a colorless liquid. As is typical for this reaction, this crude liquid was found by NMR to be contaminated with 3% of $I_2C_6H_4$ (δ_H 7.42 in $CDCl_3$) and 3% of $(Me_3Si)_2C_6H_4$ (δ_H 7.53, 0.29 in $CDCl_3$). These impurities are very difficult to separate from the desired compound by either distillation or chromatography. However, if the colorless liquid is cooled to −20 °C for 2 days *and filtered cold*, the impurity $I_2C_6H_4$ can be removed, while that of $(Me_3Si)_2C_6H_4$ can be reduced to about 1−2%. The product obtained in this fashion was used successfully in all further experiments. ^{1}H NMR (300 MHz, $CDCl_3$): δ 7.71 (part of AA′BB′ 2 H), 7.26 (part of AA′BB′ 2 H), 0.27 (s, 9H, SiMe3). ^{13}C NMR (75.4 MHz, $CDCl_3$): δ 140.0 (C_i-Si), 136.9, 135.2, 95.9(C_i-I), −1.1 ($SiCH_3$).

Combined NMR/Synthetic Scale Preparation of $p\text{-}IC_6H_4BBr_2$. In a drybox, 1.30 g (5.20 mmol) of BBr_3 was added by pipet to a solution of 1.25 g (4.51 mmol) of $p\text{-}IC_6H_4SiMe_3$ in 5−10 mL of $CDCl_3$ contained in a Schlenk flask. After the mixture was stirred for 1 min to ensure complete mixing, a 0.7 mL aliquot was transferred to an NMR tube which was subsequently sealed with several layers of Parafilm over the NMR cap. The Schlenk flask and NMR tube were placed in a 60 °C water bath, and both were removed at intervals during the course of monitoring the reaction. It took 8 h of heating for complete reaction, as is indicated by the appearance of proton resonances for $SiMe_3Br$ (δ_H 0.61) and for the desired compound $p\text{-}IC_6H_4BBr_2$ (vide infra) at the expense of resonances for $p\text{-}IC_6H_4SiMe_3$. After the reaction was complete, the volatile components were removed from the Schlenk flask by vacuum distillation at room temperature to leave 1.39 g (82%) of crude $p\text{-}IC_6H_4BBr_2$ as a nearly colorless (tannish) solid. ^{1}H NMR: δ 7.91 (part of AA′BB′), 7.86 (part of AA′BB′). ^{13}C NMR: δ 138.8, 137.8, 105.5. ^{11}B NMR: δ 56.6.

$Na[(p\text{-}IC_6H_4)B(pz)_3]$. A 100 mL Schlenk flask with a Teflon stopcock equipped with a magnetic stir bar was charged with a mixture of 1.44 g (5.23 mmol) of $p\text{-}IC_6H_4SiMe_3$ and 1.50 g (5.99 mmol) of BBr_3 and was sealed with a glass stopcock. After the flask had been subjected to a freeze−pump−thaw cycle, the

(14) Stephens, E. B.; Kinsey, K. E.; Davis, J. F.; Tour, J. M. *Macromolecules* **1993**, *26*, 3519.

apparatus was placed in a 60 °C water bath for 8 h, and then the $SiMe_3Br$ and the excess BBr_3 were removed by vacuum distillation at room temperature to leave *p*-$IC_6H_4BBr_2$ as a nearly colorless (pale pink) solid. The *p*-$IC_6H_4BBr_2$ was dissolved in 35 mL of toluene, and the solution was added via cannula to a solution of 1.07 g (15.7 mmol) of pyrazole and 1.5 mL (10.4 mmol) of NEt_3 in 100 mL of toluene. After the resulting cloudy suspension was allowed to stir at room temperature for 12 h, the toluene solution [presumably containing *p*-$IC_6H_4B(pz)_2(pzH)$] was transferred to a 500 mL Schlenk flask by cannula filtration, thereby removing the colorless precipitate of $[HNEt_3][Br]$ (1.88 g, 99%). A solution of 0.503 g (5.23 mmol) of NaO^{t}Bu in 50 mL of 1:1 toluene/THF was added via cannula to the solution of "*p*-$IC_6H_4B(pz)_2(pzH)$", the resulting suspension was stirred at 60 °C (external water bath) for 4 h, and solvent was removed by vacuum distillation. The residue was triturated with 50 mL of Et_2O, filtered, and air-dried to leave 1.00 g of the desired compound as a colorless powder. The filtrate was a 1:1 mixture of pyrazole and the desired compound (NMR); thus, solvent was removed by vacuum distillation, and the residue was triturated with 25 mL of Et_2O, filtered, and dried in an oven. The yield of the combined Et_2O-insoluble portions was 1.49 g or 65% based on $IC_6H_4SiMe_3$. Mp: 310 °C (slow dec), 328−330 °C (black liquid). ^{1}H NMR (300 MHz, CD_3OD): δ 7.55 (d, J = 1 Hz, H_3-pz, 3H), 7.49 (part of AA′BB′, 2H), 7.11 (d, J = 2 Hz, H_5-pz, 3H), 7.05 (part of AA′BB′, 2H), 6.15 (dd, J = 2,1 Hz, 3H). ^{13}C NMR (75.4 MHz, CD_3OD): δ 140.7 (C_5-pz), 137.5 (aryl), 136.8 (aryl), 135.9 (C_3-pz), 134.7 (C_i-B), 104.5 (C_4-pz), 93.2 (C_i-I). High resolution ESI(−) MS, calcd (obsd) for anion: 415.0340 (457.0351).

Na[(*p*-IC$_6$H$_4$)B(3-Mepz)$_3$]. Similar to the parent derivative above, the reaction between 2.36 g (8.56 mmol) of *p*-$IC_6H_4SiMe_3$ and 2.51 g (10.0 mmol) of BBr_3 neat was used to produce *p*-$IC_6H_4BBr_2$, which was then dissolved in situ in 50 mL of toluene. The *p*-$IC_6H_4BBr_2$ solution was added via cannula to a solution of 2.11 g (25.7 mmol) of 3-methylpyrazole and 2.4 mL (17.2 mmol) of NEt_3 in 200 mL of toluene. After the resulting cloudy suspension was allowed to stir at room temperature overnight, the toluene solution [presumably containing *p*-$IC_6H_4B(3\text{-}Mepz)_2(3\text{-}MepzH)$] was transferred to a 500 mL Schlenk flask by cannula filtration, thereby removing the colorless precipitate of $[HNEt_3][Br]$ (3.00 g, 96%). A solution of 0.823 g (8.56 mmol) of NaO^{t}Bu in 50 mL of 1:1 toluene/THF was added by cannula to the solution of "*p*-$IC_6H_4B(3\text{-}Mepz)_2(3\text{-}MepzH)$", and the resulting suspension was stirred for 12 h. The colorless solid was separated by filtration, washed with two 100 mL portions of hexanes, and dried under vacuum to leave 3.08 g (75%) of Na[(*p*-IC_6H_4)B(3-Mepz)$_3$] as a colorless solid. Mp: 310 °C (sinters), 348−350 °C (dec, black liquid with effervescence). Anal. Calcd for $C_{18}H_{19}BIN_6Na$: C, 45.03; H, 3.99; N, 17.50. Found: C, 45.30; H, 4.31; N, 17.29. ^{1}H NMR (300 MHz, CD_3OD): δ 7.46 (part of AA′BB′, 2H), 7.07 (part of AA′BB′, 2H), 6.98 (d, J = 2 Hz, H_5-pz, 3H), 5.88 (d, J = 2 Hz, H_4-pz, 3H), 2.23 (s, 9H, CH_3). ^{13}C NMR (75.4 MHz, CD_3OD): δ 149.9, 137.7, 136.8, 136.6 (aryl, C_3- and C_5-pz), 104.1 (C_4-pz), 92.9 (C−I), 13.6 (CH_3) (C−B not obsd). High resolution ESI(−) MS, calcd (obsd) for anion: 457.0812 (457.0811).

Bis{(*p*-iodophenyl)[tris(pyrazolyl)]borato}iron(II), Fe[(*p*-IC$_6$H$_4$)B(pz)$_3$]$_2$. A solution of 1.30 g (2.97 mmol) of Na[(*p*-IC_6H_4)B(pz)$_3$] in 100 mL of 1:1 MeOH:H_2O was added to 100 mL of an aqueous solution of $FeBr_2$ (0.320 g, 1.48 mmol), resulting in the immediate precipitation of a purple solid. The suspension was stirred for 30 min and filtered, and the purple solid was washed with two 50 mL portions of H_2O. The resulting solid was then taken up in CH_2Cl_2, the purple solution was dried over $MgSO_4$ and filtered, and solvent was removed to yield 1.14 g (87%) of Fe[(*p*-IC_6H_4)B(pz)$_3$]$_2$ as a purple solid. The product was dissolved in 80 mL of CH_2Cl_2 and filtered, and 160 mL of methanol was layered on the purple solution, which, after the solvents were allowed to diffuse slowly over 2 days, yielded 0.975 g (74%) of lustrous purple needles. Mp: 295−298 °C (dec, black liquid). Anal. Calcd for $C_{30}H_{26}B_2FeI_2N_{12}$: C, 40.67; H, 2.96; N, 18.97. Found: C, 40.30; H, 2.47; N,18.70. ^{1}H NMR (300 MHz, $CDCl_3$): δ 8.14, 8.05, 7.61, 6.13, 6.00.^{13}C NMR (75.4 MHz): δ 148.1 (Ar), 139.4 (Ar), 137.5 ($C_{3/5}$-pz), 105.7 (C_4-pz), 95.2 (C_i-I). High resolution MS, direct probe, calcd (obsd): 886.0039 (886.0044).

Bis{(*p*-iodophenyl)[tris(3-methylpyrazolyl)]borato}iron(II), Fe[(*p*-IC$_6$H$_4$)B(3-Mepz)$_3$]$_2$. The addition of 100 mL of an aqueous solution of 0.284 g (1.32 mmol) of $FeBr_2$ to a methanol solution of 1.27 g (2.64 mmol) of Na[(*p*-IC_6H_4)B(3-Mepz)$_3$] yielded a copious amount of colorless solid that was isolated by filtration. The solid was then taken up in CH_2Cl_2, the solution was dried over $MgSO_4$ and filtered, and the $MgSO_4$ was extracted twice with 100 mL of refluxing benzene and filtered hot. After cooling, and solvent was removed from the combined organic fractions by rotary evaporation to yield 1.03 g (80% yield) of pure Fe[(*p*-IC_6H_4)B(3-Mepz)$_3$]$_2$ as a colorless solid. Recrystallization by layering a CH_2Cl_2 solution with methanol and allowing the solvents to diffuse slowly at room temperature over 2 days yielded 0.912 g (71% yield) of X-ray-quality colorless block crystals (form I^{nSCO}, where the superscript nSCO stands for "no spin crossover"). Mp (form I^{nSCO}): 280 °C (slowly darkens); 335−338 °C (dec, red-black liquid). Anal. Calcd for $C_{36}H_{38}B_2FeI_2N_{12}$: C, 44.57; H, 3.95; N, 17.33. Found: C, 44.65; H, 3.56; N, 17.25. A second polymorph of Fe[(*p*-IC_6H_4)B(3-Mepz)$_3$]$_2$ (form II^{SCO}, "spin crossover") is formed within 20 min to 1 h at room temperature as small crystallites at the boundary between the slowly diffusing MeOH and CH_2Cl_2 layers. This second polymorph can be formed preferentially [possibly contaminated by a trace of the (desolvated) solvate, form III^{SCO}] by allowing approximately 2−4 mM CH_2Cl_2 solutions contained in 5 dram vials to evaporate in the hood (maintained at a flow rate of 80−100 ft^3/min) over a period of 8−12 h. The reproducibility of the evaporative growth of the second polymorph is somewhat problematic, as slower evaporation rates tended to lead to the formation of quantities of the first polymorph, while faster rates may lead to more of the desolvated third form. Leaving crystals of II^{SCO} in the mother liquid causes them to convert to form I^{nSCO} over time. The platelike block crystals of I^{nSCO} are resistant to redissolution in CH_2Cl_2, which is fortuitous because the "as-formed" crystalline samples may contain a small quantity of the second, more soluble polymorph II^{SCO} that can be removed by washing with a minimal quantity of CH_2Cl_2. Mp (form II^{SCO}): 250−260 °C (slowly darkens); 338−345 °C (dec, red-black liquid). Anal. Found: C, 44.43; H, 3.62; N, 17.12. If the methanol/CH_2Cl_2 crystallization is carried out at −20 °C by using a precooled apparatus, cold CH_2Cl_2 solutions, and a cold diffusing solvent, large blocks of the methylene chloride solvate, Fe[(*p*-IC_6H_4)B(3-Mepz)$_3$]$_2$·CH_2Cl_2 (III^{SCO}), are formed preferentially (ca. 78%, vide infra), where the minor impurity is the form I^{nSCO} polymorph. These crystals lose solvent and concomitantly turn opaque and fracture within seconds of exposure to air. Even though it is possible to mechanically separate the three forms as single crystals, it has not yet been possible to grow pure bulk phases of the last two forms of Fe[(*p*-IC_6H_4)B(3-Mepz)$_3$]$_2$. Mp (form III^{SCO}, air-dried, desolvated crystals): 265−275 °C (slowly darkens); 340−345 °C (dec, red-black liquid). Anal. Found: C, 44.57; H, 3.99; N, 17.24. ^{1}H NMR (300 MHz, $CDCl_3$): δ 45.8, 43.8, 4.3, 2.1, −6.3. High resolution MS, direct probe, calcd (obsd): 970.0980 (970.0526).

Crystallography. X-ray intensity data from a reddish-purple bar of Fe[(*p*-IC_6H_4)B(pz)$_3$]$_2$ and a colorless block of Fe[(*p*-IC_6H_4)B(3-Mepz)$_3$]$_2$ (form I^{nSCO}) were measured at 150(1) K, whereas those from a prism of Fe[(*p*-IC_6H_4)B(3-Mepz)$_3$]$_2$ (form II^{SCO}) were measured at 294(1) K (colorless), 200(1) K (pink), and 100(1) K (purple), and those from a boxlike crystal of Fe[(*p*-IC_6H_4)B(3-Mepz)$_3$]$_2$·CH_2Cl_2 (III^{SCO}) were measured at 200(1) K (pink) and subsequently at 100(1) K (purple) on a Bruker SMART APEX CCD-based diffractometer (Mo Kα radiation, $\lambda = 0.71073$ Å).[15] Raw data frame integration and Lp corrections were performed with SAINT+.[15] Final unit cell parameters were determined by least-squares refinement of 7428 reflections from the data set of Fe[(*p*-IC_6H_4)B(pz)$_3$]$_2$, of 7459 reflections from the data set of Fe[(*p*-IC_6H_4)B(3-Mepz)$_3$]$_2$ (form I^{nSCO}), and of 9522 reflections from the data set of Fe[(*p*-IC_6H_4)B(3-Mepz)$_3$]$_2$ (form II^{SCO}), each with $I > 5\sigma(I)$. Analyses of the data showed negligible crystal decay during all data collection. An empirical absorption correction was applied to the data sets of the first two complexes with SADABS,[15] whereas an analytical absorption correction was applied to the data of the last complex using six indexed faces, {011}, {01−1}, and {100} with XPREP.[16] A face-indexed absorption correction was applied to the last crystal due to its well-defined faces. The faces of other crystals in the paper could not be indexed, so an empirical correction was necessary. Direct methods structure solution, difference Fourier calculations, and full-matrix least-squares refinements against F^2 were performed with SHELXTL.[16]

Fe[(*p*-IC_6H_4)B(pz)$_3$]$_2$ crystallizes in the *Pbcn* space group, as determined by the pattern of systematic absences in the intensity data. Systematic absences in the intensity data indicated the $P2_1/c$ space group for each form of Fe[(*p*-IC_6H_4)B(3-Mepz)$_3$]$_2$. All three complexes are situated on crystallographic inversion centers. All non-hydrogen atoms were refined with anisotropic displacement parameters; hydrogen atoms were placed in idealized positions and included as riding atoms.

Results

Syntheses. The Fe[(*p*-IC_6H_4)B(3-Rpz)$_3$]$_2$ complexes, where R is H or Me, were prepared in good yield by the metathetical reaction between Na[(*p*-IC_6H_4)B(3-Rpz)$_3$] and iron(II) halides. The preparation of high-purity Na[(*p*-IC_6H_4)B(3-Rpz)$_3$] (R = H, Me) was critical to the success of the reaction, and a number of routes were explored. By far, the most efficient route to the compound was that depicted in Scheme 1, which was inspired by the synthesis reported both by Wagner and co-workers[17] in their preparation of ferrocenyltris(pyrazolyl)-borate compounds and by Janiak and co-workers,[18] who adapted the procedure to alkylborato derivatives.

Scheme 1. High-Yield Route to Na[(*p*-IC_6H_4)B(pz^{3R})] (R = H, Me)

$$p\text{-}I_2C_6H_4 + 2Li^tBu \xrightarrow[-78\ °C]{THF} \text{“}LiC_6H_4I\text{”} + LiI + HCMe_3 + H_2CCMe_2 \xrightarrow[\text{ii. RT, 1.5 h}]{\text{i. } SiMe_3Cl,\ -78\ °C,\ 1\ h} Me_3SiC_6H_4I + LiCl \quad (A)$$

$$Me_3SiC_6H_4I + 1.2BBr_3 \xrightarrow[60\ °C,\ 8\ h]{\text{neat or } CDCl_3} IC_6H_4BBr_2 + SiMe_3Br \quad (B)$$

$$IC_6H_4BBr_2 + \underset{(R = H, Me)}{3Hpz^{3R}} + 2NEt_3 \xrightarrow[-2[HNEt_3][Br]]{toluene} IC_6H_4B(pz^{3R})_2(Hpz^{3R}) \xrightarrow[-HO^tBu]{+NaO^tBu} [Na][IC_6H_4B(pz^{3R})_3] \quad (C)$$

Each step in Scheme 1 requires comment, as deviations from the described protocol severely undermine the reproducibility of the syntheses. The preparation of *p*-$IC_6H_4SiMe_3$ followed a modification of Tour's procedure.[14] In the current modification, it was found necessary to keep the reaction mixture of "LiC_6H_4I" at −78 °C until after an excess of $SiMe_3Cl$ has been added and the mixture had been stirred for a short period of time. If the mixture is allowed to warm to room temperature, even momentarily, and is then recooled before the addition of $SiMe_3Cl$, significant quantities of soluble oligo- or polyphenylene products are formed. Even with the above modification, the product obtained after flash chromatography (SiO_2/hexanes) was frequently contaminated with minor quantities (5−10%) of $I_2C_6H_4$ and/or $(Me_3Si)_2C_6H_4$. These impurities conveniently crystallize from *p*-$IC_6H_4SiMe_3$ when the mixture is held at −20 °C and can be separated by filtration. The preparation of *p*-$IC_6H_4BBr_2$ was achieved by exploiting the well-known reactions between boron trihalides and trimethylsilyl aryls.[19,20] Unlike these latter reactions, in which complete conversion to $ArBX_2$ (X = Cl, Br) is fairly rapid and occurs at or below room temperature, the preparation of *p*-$IC_6H_4BBr_2$ diluted in $CDCl_3$ required 8 h of heating for a complete reaction, as determined by an NMR study. Further studies showed that more concentrated samples reacted within 1.5 h at 60 °C. Finally, the choice of toluene as a solvent is critical to the success of the subsequent reaction between *p*-$IC_6H_4BBr_2$ and pyrazole, because it was found in separate experiments that the use of THF resulted in products derived from cleavage of the furan ring.

Attempts to prepare the Na[(*p*-IC_6H_4)B(pz^{3R})$_3$] compounds by alternative routes using the potentially attractive reagent *p*-$IC_6H_4B(OH)_2$, which is commercially available and air stable, were also investigated, but mixtures were always obtained. Thus, the reaction between *p*-$IC_6H_4B(OH)_2$, pyrazole, and sodium/potassium pyrazolide[21] gave M[(*p*-IC_6H_4)B(3-Rpz)$_3$] (M = Na, K; R = H, Me), contaminated with boroxine [*p*-$IC_6H_4B(\mu\text{-}O)]_3$ or its pyrazolyl adducts [(*p*-IC_6H_4)B(μ-O)]$_3$·(Hpz^{3R}) (R = H, Me).[22] The reaction between *p*-$IC_6H_4B(OH)_2$ and $LiAlH_4$ [giving $Li(THF)_n$[(*p*-IC_6H_4)BH_3 (n = 1−3)],[23] followed by reaction with the

(15) *SMART, Version 5.625, SAINT+, Version 6.22, and SADABS, Version 2.05*; Bruker Analytical X-ray Systems, Inc.: Madison, WI, 2001.
(16) Sheldrick, G. M. *SHELXTL, Version 6.1*; Bruker Analytical X-ray Systems, Inc.: Madison, WI, 2000.
(17) Jäkle, F.; Polborn, K.; Wagner, M. *Chem. Ber.* **1996**, *129*, 603.
(18) Janiak, C.; Braum, L.; Girgsdies, F. *J. Chem. Soc., Dalton Trans.* **1999**, 3133.
(19) (a) Kaufmann, D. *Chem. Ber.* **1987**, *120*, 853. (b) Kaufmann, D. *Chem. Ber.* **1987**, *120*, 901. (c) Gross, U.; Kaufmann, D. *Chem. Ber.* **1987**, *120*, 991. (d) Rottlander, M.; Palmer, N.; Knochel, P. *Synlett* **1996**, 573. (e) Hupe, E.; Calaza, M. I.; Knochel, P. *Chem. Commun.* **2002**, 1390.
(20) Haubold, W.; Herdtle, J.; Gollinger, W.; Einholz, W. *J. Organomet. Chem.* **1986**, *315*, 1.
(21) White, D.; Faller, J. W. *J. Am. Chem. Soc.* **1982**, *104*, 1548.
(22) Similar to (a) [PhB(μ-O)]$_3$·(Hpz): Niedenzu, K.; Bielawski, J. *Inorg. Chem.* **1986**, *25*, 1771. Niedenzu, K.; Bielawski, J. *Inorg. Chem.* **1986**, *25*, 85. (b) [PhB(μ-O)]$_3$·(7-azaindole): Wu, Q. G.; Wu, G.; Brancaleon, L.; Wang, S. *Organometallics* **1999**, *18*, 2553. (c) [PhB(μ-O)]$_3$·(py): Beckmann, J.; Dakternieks, D.; Duthie, A.; Lim, A. E. K.; Tiekink, E. R. T. *J. Organomet. Chem.* **2001**, *633*, 149.
(23) Kisko, J. L.; Haseall, T.; Kimblin, C.; Parkin, G. *J. Chem. Soc., Dalton Trans.* **1999**, 1929.

Table 1. Crystallographic Data for Fe[(*p*-IC$_6$H$_4$)B(pz)$_3$]$_2$, Fe[(*p*-IC$_6$H$_4$)B(3-Mepz)$_3$]$_2$ (Form I^{n}SCO), Fe[(*p*-IC$_6$H$_4$)B(3-Mepz)$_3$]$_2$ (Form II^{SCO}), and Fe[(*p*-IC$_6$H$_4$)B(3-Mepz)$_3$]$_2$·CH$_2$Cl$_2$ (Form III^{SCO})

	Fe[(IC$_6$H$_4$)B(3-Rpz)$_3$]$_2$						
	R = H	R = Me					
		form I^{n}SCO	form II^{SCO}	form II^{SCO}	form II^{SCO}	form III^{SCO} (2CH$_2$Cl$_2$)	form III^{SCO} (2CH$_2$Cl$_2$)
empirical formula	C$_{30}$H$_{26}$B$_2$-FeI$_2$N$_{12}$	C$_{36}$H$_{38}$B$_2$-FeI$_2$N$_{12}$	C$_{36}$H$_{38}$B$_2$-FeI$_2$N$_{12}$	C$_{36}$H$_{38}$B$_2$-FeI$_2$N$_{12}$	C$_{36}$H$_{38}$B$_2$-FeI$_2$N$_{12}$	C$_{38}$H$_{42}$B$_2$Cl$_4$-FeI$_2$N$_{12}$	C$_{38}$H$_{42}$B$_2$Cl$_4$-FeI$_2$N$_{12}$
formula wt	885.90	970.05	970.05	970.05	970.05	1139.91	1139.91
temperature (K)	150(1)	150(1)	294(1)	200(1)	100(1)	200(1)	100(1)
space group	*Pbcn*	*P*2$_1$/*c*	*P*2$_1$/*c*	*P*2$_1$/*c*	*P*2$_1$/*c*	*P*2$_1$/*c*	*P*2$_1$/*c*
a (Å)	18.0250(9)	11.1677(6)	11.0501(5)	10.7587(5)	10.4732(5)	12.0760(7)	11.8468(7)
b (Å)	8.7070(4)	13.0473(7)	15.7119(7)	15.7861(8)	15.8022(7)	14.6548(9)	14.5537(9)
c (Å)	20.7543(10)	13.1043(7)	11.8054(5)	11.6703(6)	11.5601(5)	12.7920(8)	12.7124(8)
α (°)	90	90	90	90	90	90	90
β (°)	90	90.0800(10)	102.9270(10)	102.0760(10)	101.1200(10)	93.5690(10)	93.3170(10)
γ (°)	90	90	90	90	90	90	90
volume (Å^3)	3257.3(3)	1909.40(18)	1997.68(15)	1938.20(17)	1877.27(15)	2259.4(2)	2188.1(2)
Z	4	2	2	2	2	2	2
ρ_{calcd} (g/cm^3)	1.807	1.687	1.613	1.662	1.716	1.676	1.730
abs. coeff. (mm^{-1})	2.402	2.057	1.966	2.026	2.092	1.980	2.045
final *R* indices [$I > 2\sigma(I)$]	R1 = 0.0337, wR2 = 0.0750	R1 = 0.0272, wR2 = 0.0726	R1 = 0.0366, wR2 = 0.0954	R1 = 0.0355, wR2 = 0.0831	R1 = 0.0275, wR2 = 0.0662	R1 = 0.0318, wR2 = 0.0772	R1 = 0.0272, wR2 = 0.0663

desired pyrazoles, produced intractable mixtures of Li[B(3-Mepz)$_4$], Li[HB(3-Rpz)$_3$], and trace amounts of Li[(*p*-IC$_6$H$_4$)B(3-Rpz)$_3$]. In either route, the yields of the desired products suffered poor reproducibility and never exceeded 25%. ^{1}H NMR spectra of violet Fe[(*p*-IC$_6$H$_4$)B(pz)$_3$]$_2$ in CDCl$_3$ showed broadened resonances in the 8−6 ppm range, indicating a LS diamagnetic complex at room temperature. The broadened nature of the resonances is attributed to a paramagnetic impurity, possibly a result of the slow decomposition of the complex in CDCl$_3$. In contrast, the ^{1}H NMR spectra of colorless CDCl$_3$ solutions of Fe[(*p*-IC$_6$H$_4$)B(3-Mepz)$_3$]$_2$ exhibit broad resonances in the range of −6 to 50 ppm, a range that is indicative of the HS, paramagnetic nature of this complex in solution.

Solid State Structures. The Fe[(*p*-IC$_6$H$_4$)B(3-Rpz)$_3$]$_2$ (R = H, Me) complexes can be obtained as exquisite crystals by layering CH$_2$Cl$_2$ solutions with MeOH and allowing the solvents to slowly diffuse. The crystallizations are best performed in the absence of light (foil-covered vials were used in the present case), which prevents the solutions from turning either brown when R is H or orange when R is Me as a result of the formation of unidentified iron(III) impurities (as is revealed by Mössbauer spectroscopy in the latter case).

Simple inspection of the color of the crystals can be used as a first indication of the spin states of the iron(II) poly(pyrazolyl)borate complexes because the LS complexes are purple whereas the HS complexes are colorless. In the case of Fe[(*p*-IC$_6$H$_4$)B(3-Rpz)$_3$]$_2$, the R = H derivative is purple, whereas the R = Me derivative is colorless at room temperature. Once formed, the crystals of each derivative are resistant to redissolution in CH$_2$Cl$_2$ and exhibit only modest solubility in CDCl$_3$. The as-formed powders of these complexes exhibit much greater solubility.

The electron configurations of the iron(II) poly(pyrazolyl)borate complexes can be readily determined from the Fe−N bond distances in the solid-state structures because the population of the antibonding e$_g$* orbitals in HS $t_{2g}^4e_g^{*2}$ complexes causes the Fe−N bond distances to be ca. 0.2 Å longer than in LS $t_{2g}^6e_g^{*0}$ complexes. Because the bite angles of tris(pyrazolyl)borate ligands are generally fixed, there are other subtle distortions of the ligand framework that occur on binding to metals of different size. We have previously noted[12g] in tris(pyrazolyl)methane iron(II) complexes that the extent of tilting of the pyrazolyl rings from ideal C_{3v} symmetry depends largely upon the size of the metal, and thus the spin state of the iron(II) complexes. The M−N(*n*1)−N(*n*2)−B and the M−N(*n*1)−N(*n*2)−C(*n*1) torsion angles (see Figure 1), where *n* is the pyrazolyl ring number, describe the degree of ligand tilting. This tilting is best visualized in the bottom right views of Figures 1 and 4, which show the molecules oriented down the pseudo-three-fold axis. When these ligands are bound to smaller metal ions, e.g., LS iron(II), the M−N−N−B and M−N−N−C torsion angles approach their ideal values of 0° and 180°, respectively. When the ligands bind larger metal ions, e.g., HS iron(II), the M−N−N−B angle increases and the M−N−N−C angle decreases in magnitude.

The X-ray structural study of Fe[(*p*-IC$_6$H$_4$)B(pz)$_3$]$_2$ showed it was LS in the solid state. The ORTEP diagram of Fe[(*p*-IC$_6$H$_4$)B(pz)$_3$]$_2$ is given in Figure 1, and selected bond distances and angles are given in Table 2. The average Fe−N bond distance was found to be 1.98 Å, and the average Fe−N−N−C and Fe−N−N−B torsion angles are 173° and 5°, respectively. The short Fe−N bond distance and the torsion angles are consistent with the related LS iron(II) pyrazolylborate compounds, such as Fe[PhB(pz)$_3$]$_2$ (1.99 Å, 171°/5°) and Fe[pzB(pz)$_3$]$_2$ (1.97 Å, 174°/2.4°).[24]

The supramolecular structure of Fe[(*p*-IC$_6$H$_4$)B(pz)$_3$]$_2$, shown in Figure 2, is that of corrugated sheets. The corrugated sheets result from two types of CH−π interactions and a set of π−π interactions. The molecules of Fe[(*p*-IC$_6$H$_4$)B(pz)$_3$]$_2$ are arranged in chains that are oriented along *b* by one set of CH−π interactions between the acidic hydrogens H(12) at the 4-position of the pyrazolyl ring of

(24) Sohrin, Y.; Kokusen, H.; Matsui, M. *Inorg. Chem.* **1995**, *34*, 3928.

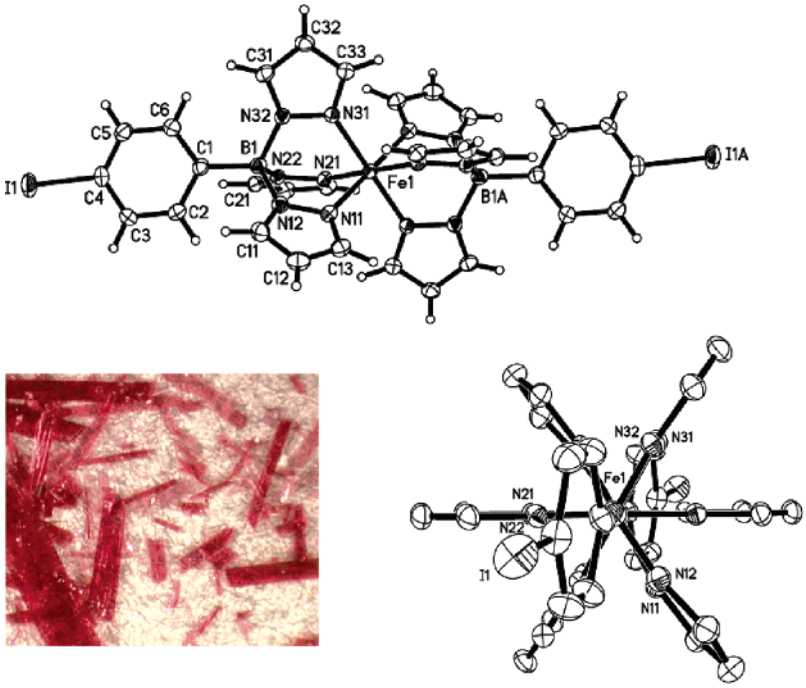

Figure 1. View of crystals (bottom left) and ORTEP diagrams of Fe[(*p*-IC_6H_4)B$(pz)_3]_2$ showing atom labeling (top) and (bottom right) a view emphasizing the Fe−N−N−C torsion angles. Thermal ellipsoids are drawn at the 50% probability level.

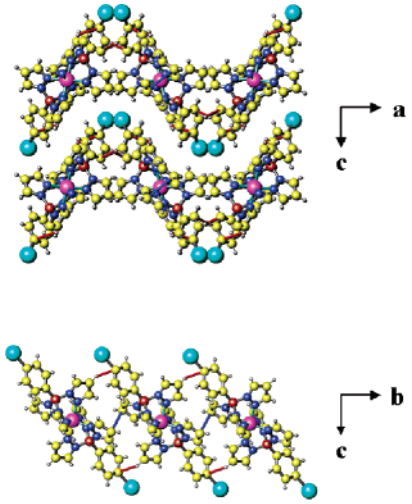

Figure 2. Supramolecular structure of Fe[(*p*-IC_6H_4)B$(pz)_3]_2$. (Top) View depicting stacking of corrugated sheets held together by $\pi-\pi$ (blue lines) and CH$-\pi$ interactions (red lines). (Bottom) View showing the stacking along the *b* axis as a result of CH$-\pi$ (red lines) and $\pi-\pi$ (blue lines) interactions.

one borate ligand and the π-cloud of a neighboring iodophenyl ring {CH(12)−arene centroid distance (Ct) of 3.29 Å, CH(12)−arene centroid angle of 126.5°} working in tandem with a $\pi-\pi$ interaction involving neighboring pyrazolyl rings that contain N(11) {centroid−centriod distance (Ct[N(11)]−Ct[N(11)]) of 3.87 Å, perpendicular interplane separation of 3.44 Å, parallel arene planes with a slip angle between plane centroids, β, of 27.3°}. The chains are connected in a second dimension to form a sheet as a result of a second set of CH$-\pi$ interactions between neighboring iodophenyl substituents [CH(5)−Ct(arene) 3.42 Å, 155.4°]. The geometry of each type of interaction is within typical values.[25] There are no unusually short interatomic distances between the sheets; they are bound by simple van der Waals interactions.

The Fe[(*p*-IC_6H_4)B$(3\text{-Mepz})_3]_2$ complex crystallizes in any one of three colorless forms, depending on the crystallization conditions (see Experimental Section). Two of the forms are polymorphs (forms I^{nSCO} and II^{SCO}), whereas the third form (III^{SCO}) is a methylene chloride solvate. A comparison of the unit cell parameters and other details of the three crystalline forms of Fe[(*p*-IC_6H_4)B$(3\text{-Mepz})_3]_2$ is summarized in Table 1. Because the first two crystalline forms were originally visually indistinguishable at room temperature, it was fortunate that these polymorphs were easily distinguishable at lower temperatures, as is illustrated in Figure 3. Polymorph I^{nSCO} remains colorless (or pale blue-green) upon cooling to 78 K, whereas polymorph II^{SCO} changes from colorless to violet upon cooling to 78 K, a change that is indicative of a change of spin state of the iron(II) ion. Crystals of form III^{nSCO} slowly turn violet as the temperature is lowered.

Single-crystal X-ray structural studies of each form of Fe[(*p*-IC_6H_4)B$(3\text{-Mepz})_3]_2$ revealed that the iron(II) ions are HS at the highest temperatures at which diffraction data were collected, i.e., 150, 294, and 200 K for I^{nSCO}, II^{SCO}, and III^{SCO}, respectively. Due to rapid desolvation even when encased in a protective coat of epoxy resin, crystals of form III^{SCO} did not survive data collection at temperatures above 200 K. Figure 4 shows a numbered ORTEP for form I^{nSCO} as well as a view emphasizing the Fe−N−N−C torsion angles. The average iron−nitrogen bond distances are 2.18, 2.18, and 2.16 Å for forms I^{nSCO}, II^{SCO}, and III^{SCO}, respectively.

(25) (a) Takahashi, H.; Tsuboyama, S.; Umezawa, Y.; Honda, K.; Nishio, M. *Tetrahedron* **2000**, *56*, 6185. (b) Janiak, C. *J. Chem. Soc., Dalton Trans.* **2000**, 3885. (c) Reger, D. L.; Gardinier, J. R.; Semeniuc, R. F.; Smith, M. D. *J. Chem. Soc., Dalton Trans*. **2003**, 1712.

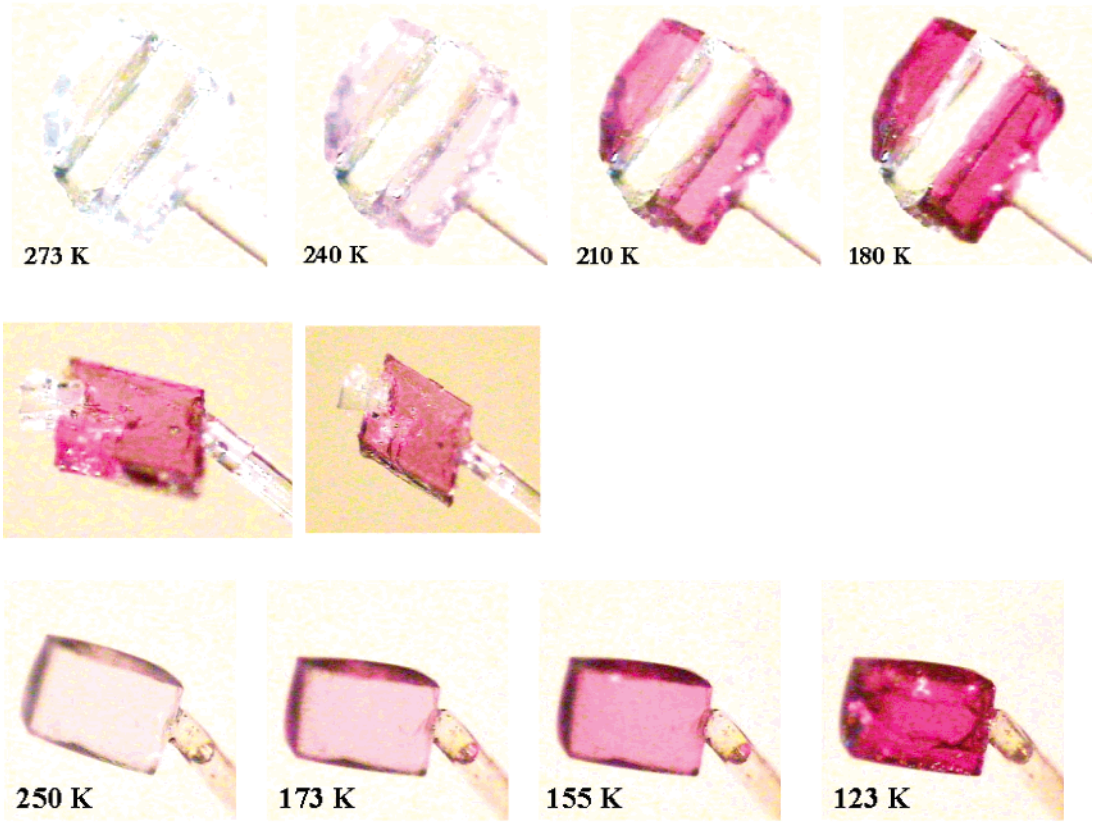

Figure 3. (Top) Temperature dependence of the crystal color of the two polymorphs of Fe[(*p*-IC$_6$H$_4$)B(3-Mepz)$_3$]$_2$ alternately epoxied on a glass fiber. (Middle) As-grown intergrowth twin aggregation of form I^{nSCO} (colorless) and form II^{SCO} (purple) at 150 K. (Bottom) Temperature dependence of the crystal color for the CH_2Cl_2 solvate of Fe[(*p*-IC$_6$H$_4$)B(3-Mepz)$_3$]$_2$.

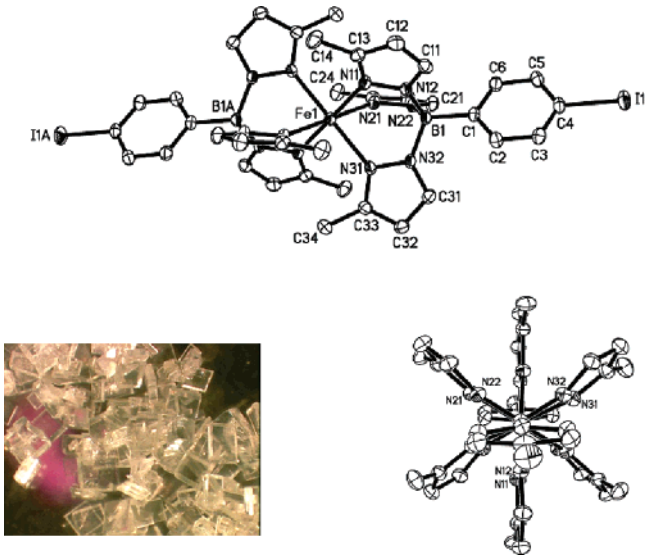

Figure 4. View of crystals (bottom left) and ORTEP diagrams of Fe[(*p*-IC$_6$H$_4$)B(3-Mepz)$_3$]$_2$ showing atom labeling (top) and a view emphasizing the Fe−N−N−C torsion angles (bottom right). Thermal ellipsoids are drawn at the 50% probability level, and hydrogen atoms have been removed for clarity.

These distances can be compared with the average Fe−N distances found for other HS iron(II) borate complexes, such as the 2.20 Å distance found[26] in Fe[HB(3-Mepz)$_3$]$_2$, and contrasted with the 1.96 Å average Fe−N distance found in the LS Fe[(*p*-IC$_6$H$_4$)B(pz)$_3$]$_2$ complex. Moreover, the average Fe−N−N−C and Fe−N−N−B torsion angles observed for Fe[(*p*-IC$_6$H$_4$)B(3-Mepz)$_3$]$_2$ are 165 and 9° for form I^{nSCO}, 166 and 9° for form II^{SCO}, and 164 and 10° for form III^{SCO}. In contrast, these angles are 173 and 5° in the LS Fe[(*p*-IC$_6$H$_4$)B(pz)$_3$]$_2$ complex. The torsion angles in the HS complexes are much smaller than the 177 and 178° angles observed for the two crystallographically independent HS iron(II) sites found[26] in Fe[HB(3-Mepz)$_3$]$_2$. The steric interactions involving the hydrogens at the 5-position of the pyrazolyl rings and the atoms of the aryl group in complexes with the [(*p*-IC$_6$H$_4$)B(3-Mepz)$_3$]$^-$ moieties direct the deformation of the ligands such that the pyrazolyl rings *must tilt* to accommodate binding to a larger metal ion compared to the HS iron(II) complex of HB(3-Mepz)$_3$, whose ligands deform in other ways (about the boron, for instance).

Variable-temperature studies revealed the spin-crossover behavior of forms II^{SCO} and III^{SCO}. It should be noted that, in the case of the higher temperature structures of II^{SCO}, the displacement ellipsoids for the iodine atoms are abnormally large and elongated perpendicular to the plane of the phenyl ring (Figure 5). The ring carbon ellipsoids near the iodine atom (especially C4) also show a similar elongation. This elongation can be attributed to a slight positional disorder of the −C$_6$H$_4$I group at higher temperatures, a displacement that becomes more pronounced at the molecule's extremity. A two-component disorder model was used for optimal refinement of this structural disorder. As can be seen, this

(26) Calogero, S.; Lobbia, G. G.; Cecchi, P.; Valle, G.; Friedl, J. *Polyhedron* **1994**, *13*, 87.

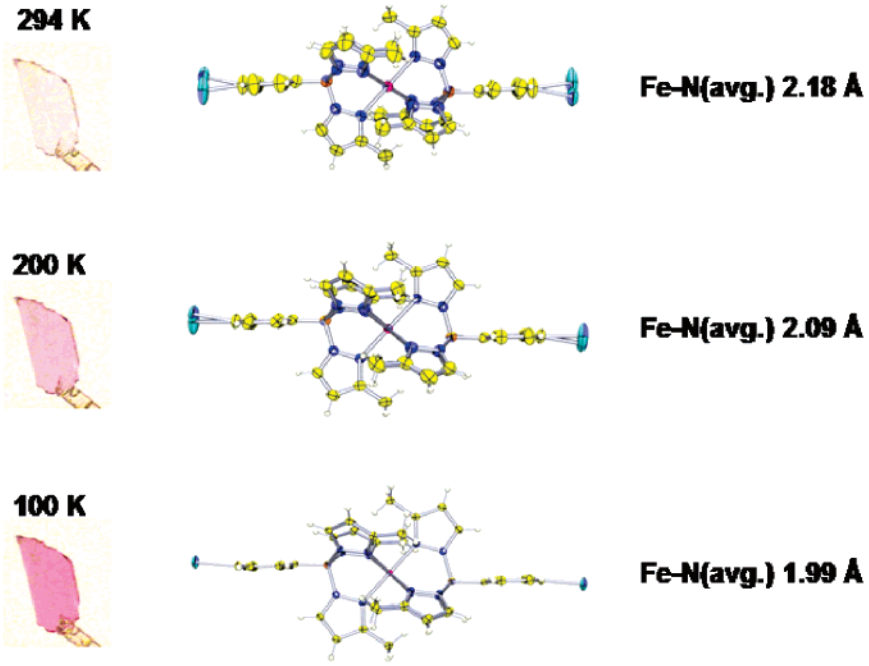

Figure 5. Changes in the crystal color, molecular structure, and Fe−N bond lengths of form II^{SCO} of Fe[(*p*-IC$_6$H$_4$)B(3-Mepz)$_3$]$_2$ at different temperatures.

Table 2. Selected Bond Lengths and Angles for Fe[(*p*-IC$_6$H$_4$)B(pz)$_3$]$_2$ and Fe[(*p*-IC$_6$H$_4$)B(3-Mepz)$_3$]$_2$ (Forms I^{n}SCO, II^{SCO}, and III^{SCO})

	Fe[(IC$_6$H$_4$)B(3-Rpz)$_3$]$_2$						
	R = H	R = Me					
		form I^{n}SCO	form II^{SCO}	form II^{SCO}	form II^{SCO}	form III^{SCO}	form III^{SCO}
temperature	150 K	150 K	294 K	200 K	100 K	200 K	100 K
			Bond Distances (Å)				
Fe−N(11)	1.963(2)	2.137(2)	2.124(2)	2.049(2)	1.967(2)	2.188(2)	2.002(2)
Fe−N(21)	1.952(2)	2.206(2)	2.207(2)	2.109(2)	2.009(2)	2.137(2)	1.9804(19)
Fe−N(31)	1.974(2)	2.208(2)	2.195(2)	2.097(2)	2.000(2)	2.162(2)	1.9953(19)
			Bond Angles (°)				
N(11)−Fe(1)−N(21)	88.22(10)	85.18(6)	85.37(7)	87.40(8)	89.39(8)	85.79(9)	89.24(8)
N(21)−Fe(1)−N(31)	88.09(10)	87.63(6)	88.46(7)	89.18(8)	89.99(8)	84.91(9)	89.27(8)
N(31)−Fe(1)−N(11)	88.63(10)	85.07(6)	85.00(7)	87.07(8)	89.56(8)	88.10(9)	89.95(8)
N(11a)−Fe(1)−N(11)	180	180	180	180	180	180	180
N(21a)−Fe(1)−N(21)	180	180	180	180	180	180	180
N(31a)−Fe(1)−N(31)	180	180	180	180	180	180	180
N(11)−Fe(1)−N(21a)	91.78(10)	94.82(6)	94.63(7)	92.60(8)	90.61(8)	94.21(9)	90.76(8)
N(21)−Fe(1)−N(31a)	91.91(10)	92.37(6)	91.54(7)	90.82(8)	90.01(8)	95.09(9)	90.73(8)
N(31)−Fe(1)−N(11a)	91.37(10)	94.93(6)	95.00(7)	92.93(8)	90.44(8)	91.90(9)	90.05(8)

"disorder" is alleviated at lower temperatures. Over the studied temperature range, the average Fe−N bond distances and torsion angles are not affected by the treatment and subsequent refinement of the disorder. On lowering the temperature to 200 K, the crystal of form II^{SCO} turns pink (middle of Figure 5), and the observed average Fe−N bond distance of 2.09 Å is intermediate between the typical HS and LS Fe−N distances of 2.20 and 1.98 Å, respectively, indicative of a significant population of the LS state in the crystal at this temperature. The associated average Fe−N−N−C and Fe−N−N−B torsion angles are 169 and 7°. Upon a further lowering of the temperature to 100 K, the crystal becomes purple, the average Fe−N distance is 1.99 Å, and the associated average Fe−N−N−C and Fe−N−N−B torsion angles are 172 and 5°, indicating both that the fraction of HS iron(II) is negligible in the crystal at this temperature and that the spin transition is complete or nearly complete. Likewise, the 100 K structure of form III^{SCO} shows a shorter Fe−N bond distance of 1.99 Å and more "ideal" Fe−N−N−C and Fe−N−N−B torsion angles of 171 and 5° than at 200 K, indicating that it has changed over to the LS form at this temperature.

A comparison of the highest temperature, HS supramolecular structures of the polymorphs of Fe[(*p*-IC$_6$H$_4$)B(3-Mepz)$_3$]$_2$ is provided in Figure 6. Overall, the supramolecular structure of I^{n}SCO is that of tightly stacked planar sheets, whereas the other two forms are made up of loosely packed corrugated sheets. The first polymorph, I^{n}SCO, crystallizes with a highly ordered three-dimensional supramolecular structure organized by weak CH−π and CH···I interactions[25,28] between neighboring molecules of Fe[(*p*-IC$_6$H$_4$)B(3-Mepz)$_3$]$_2$. As may be seen in the bottom left of Figure 6,

(27) Cecchi, P.; Berrottoni, M.; Giorgetti, M.; Calogero, S.; Lobbia, G. G.; Stievano, L. *Inorg. Chim. Acta* **2001**, *318*, 67.
(28) Ugozzoli, F.; Arduini, A.; Massera, C.; Pochini, A.; Secchi, A. *New J. Chem.* **2002**, *26*, 1718.

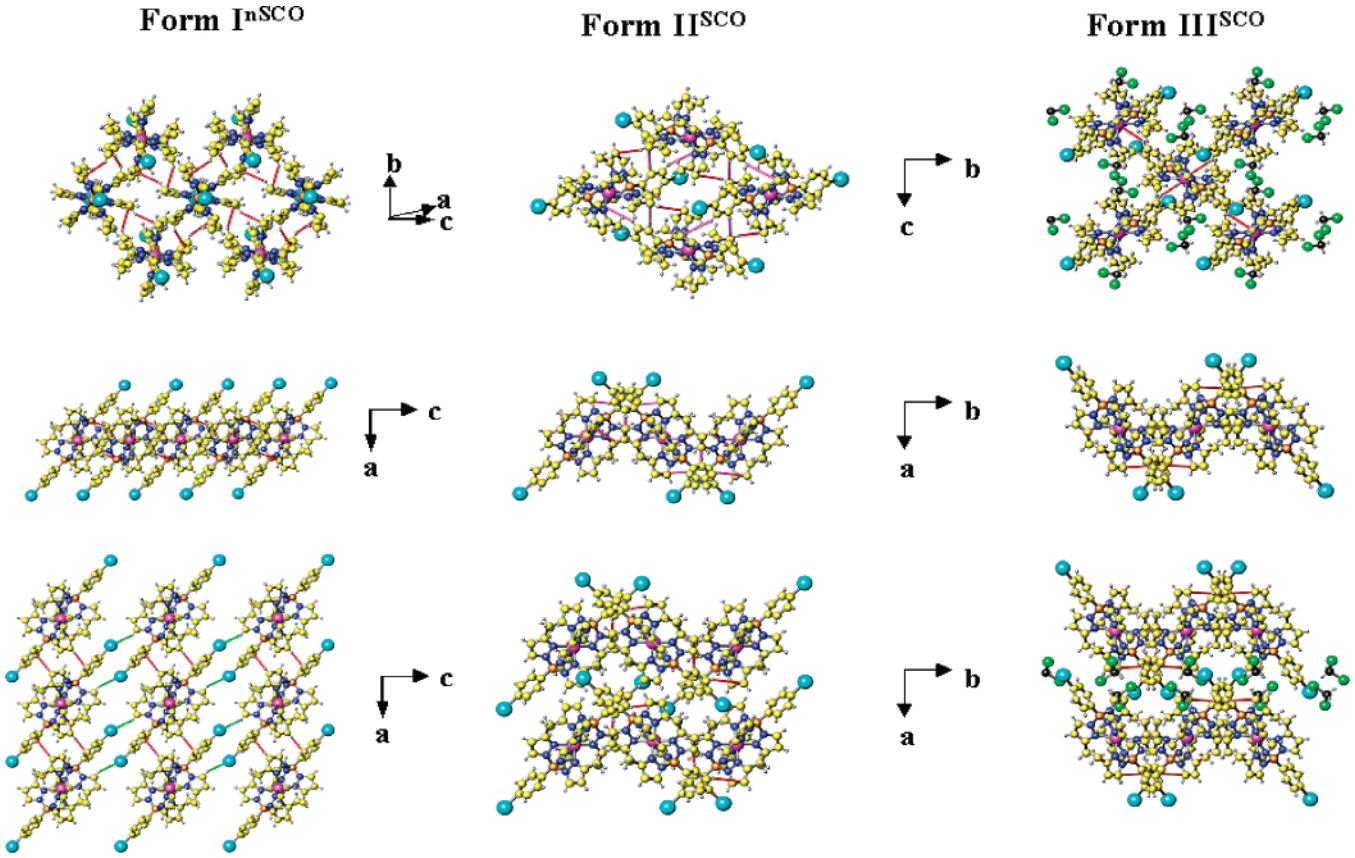

Figure 6. Comparison of the supramolecular structures of the HS forms I^{nSCO} (left), II^{SCO} (center), and III^{SCO} (right) of Fe[(*p*-IC$_6$H$_4$)B(3-Mepz)$_3$]$_2$. Crystals of form I^{nSCO} have a three-dimensional supramolecular structure based on CH$-\pi$ interactions (red lines) that form sheets and on CH$\cdots$I interactions (green lines) that hold sheets together. Crystals of forms II^{SCO} and III^{SCO} have two-dimensional corrugated sheet structures based on CH$-\pi$ interactions (red lines), and there are no short contacts between adjacent sheets.

a CH$-\pi$ interaction between the acidic hydrogen at the 4-position of a pyrazolyl ring and the π-electron cloud of a neighboring C$_6$H$_4$I ring organizes the molecules into polymeric chains along the *a*-axis [CH(22)$-$Ct 3.05 Å, 122.0°], whereas short CH$\cdots$I interactions[28] between the halogen and the acidic hydrogen at the 5-position of the pyrazolyl ring of a neighboring molecule [CH(11)$\cdots$I: 3.14 Å, 142.3°] further organize the chains into sheets in the *ac*-plane. It should be noted that the closest iodine$-$iodine distance is 4.79 Å, which is much larger than 3.96 Å, twice the van der Waals radius of iodine. As is best seen in the top drawing in Figure 6, additional CH$-\pi$ interactions involving the methyl group hydrogens H(14b) and H(24c) and the π-clouds of the pyrazolyl rings that contain N(31) and N(11), respectively {CH(14b)$-$Ct[N(31)], 3.37 Å, 147.6°; CH-(24c)$-$Ct[N(11)], 3.23 Å, 141.1°}, help to form sheets in the *bc*-plane, thereby providing cohesion of the overall supramolecular structure in three dimensions.

The second polymorph, II^{SCO}, crystallizes as loosely stacked corrugated sheets, as is shown in the middle of Figure 6, and exhibits a packing arrangement similar to that observed in the Fe[(*p*-IC$_6$H$_4$)B(pz)$_3$]$_2$ complex. In this case, however, the sheets are found in the *bc*-plane as a result of three sets of CH$-\pi$ interactions, one involving CH(22) of a pyrazolyl ring directed to the π-cloud of a second pyrazolyl ring containing N(21) {CH(22)$-$Ct[N(21)] 3.15 Å, 126.6°} and two interactions involving H(5) and H(6) of the iodophenyl group which interact with the π-clouds of the pyrazolyl rings containing N(31) and N(11), respectively {CH(5)$-$Ct[N(31)], 3.18 Å, 168.0°; CH(6)$-$Ct[N(11)], 3.30 Å, 152.2°}. The corrugated sheets, shown edge-on in the middle of Figure 6, stack along the *a*-axis, but with no unusually short interatomic distances.

Crystals of III^{SCO} exhibit a loosely stacked corrugated sheet structure (see the right portion of Figure 6) that is similar to form II^{SCO}, but in this case, the sheets are organized by only one rather than three sets of CH$-\pi$ interaction. In these crystals, the symmetry operations on the interacting asymmetric units permit the interaction to propagate in more than one dimension. This set of CH$-\pi$ interactions, which occur between phenyl group hydrogen donors and the π-clouds of the pyrazolyl rings containing N(11) {CH(45)$-$Ct[N(11)], 3.38 Å and 142.7°}, are near the upper limit for such interactions.[25] Solvent molecules reside in the voids produced by the loose packing arrangement of molecules both between and within the sheet structure.

Magnetic Studies. The temperature dependence of the effective magnetic moment was measured for bulk crystalline samples of Fe[(*p*-IC$_6$H$_4$)B(3-Mepz)$_3$]$_2$ grown under the three distinct crystallization conditions mentioned earlier, and the temperature dependence of the inverse molar magnetic susceptibility and μ_{eff} for each is shown in Figure 7. At room temperature, the observed magnetic moments for I^{nSCO}, II^{SCO}, and the desolvated crystals of III^{SCO} are 5.1, 5.2, and 5.0 μ_B,

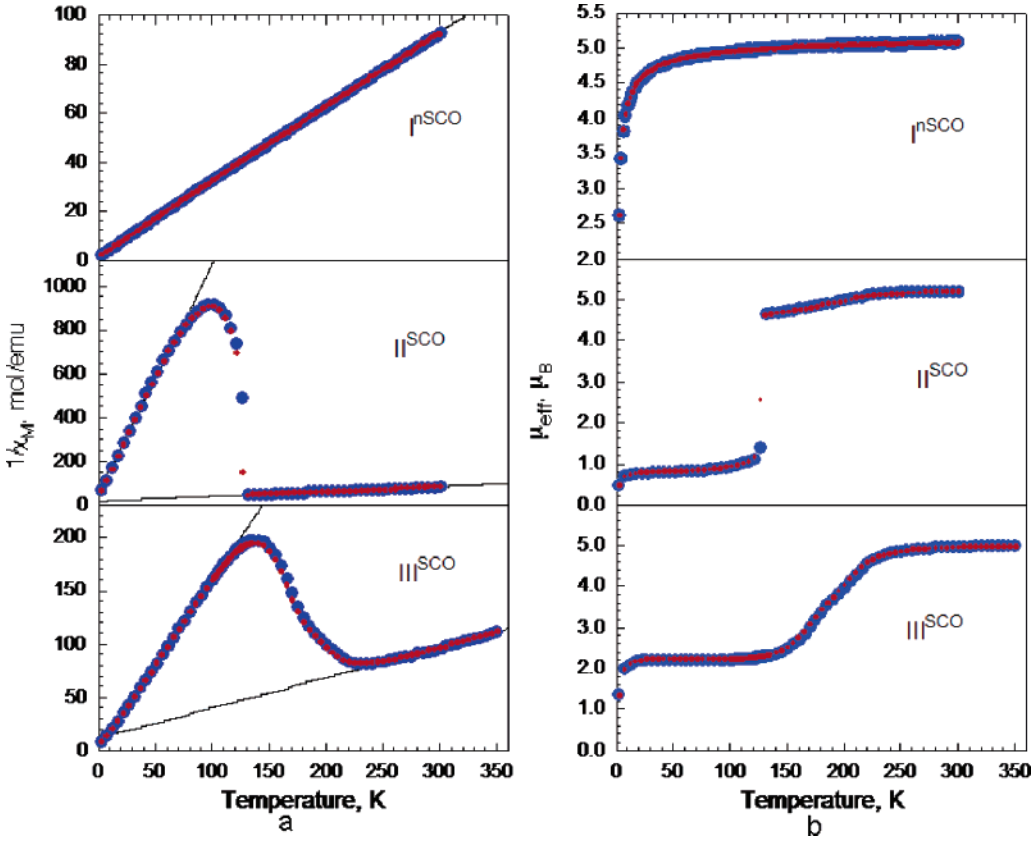

Figure 7. Plots of the (a) inverse molar magnetic susceptibility and (b) effective magnetic moment versus temperature for I^{nSCO}, II^{SCO}, and the desolvated crystals of III^{SCO}.

respectively. These moments are slightly higher than the spin-only moment of 4.9 μ_B expected for a HS iron(II) complex and indicate the expected[31] presence of a small orbital contribution to the moment. These room-temperature moments are also in good agreement with the moments observed in related HS iron(II) complexes such as Fe[HB(3,5-Me_2-pz)$_3$]$_2$ and Fe[HB(3,4,5-Me_3pz)$_3$]$_2$, which exhibit[10b−d] moments of 5.0 and 5.2 μ_B at 298 K, respectively, {Fe[2,6-di(pyrazol-3-yl)pyridine]$_2$}[Fe(CN)$_5$(NO)], which exhibits[11a] a moment of 5.4 μ_B at 298 K, and {Fe[2,6-di(pyrazol-1-yl)-pyridine]$_2$}[ClO_4]$_2$(CH_3CN), which exhibits[11b] a moment of ca. 5.5 μ_B at 298 K.

Upon cooling of the sample, the magnetic moment of I^{nSCO} decreases slightly from 5.0 μ_B at 295 K to ca. 4.8 μ_B at 50 K, and then decreases more substantially below ca. 40 K. However, as may be seen in Figure 7a, $1/\chi$ versus T is linear even at the lowest temperatures. The decrease in the moment below ca. 40 K is exactly that expected[31,32] of a magnetically dilute HS iron(II) complex in a highly distorted octahedral coordination environment. Thus, the decrease in moment at the lowest temperatures is not associated with any change in the spin state of the iron(II) ion, i.e., I^{nSCO} is a HS paramagnetic iron(II) complex at all temperatures above 4 K.

In contrast to the behavior of I^{nSCO}, as may be seen in Figure 7b, the magnetic moment of II^{SCO} slowly decreases to 4.7 μ_B upon cooling until, at ca. 131 K, the moment abruptly decreases to 1.0 μ_B at 121 K; the moment then decreases to a constant value of about 0.8 μ_B on further cooling. The residual moment of ca. 0.8 μ_B is due to both some temperature-independent paramagnetism[10] and the presence of traces of either some HS iron(II) or HS iron(III) impurity. If one assumes a 500×10^{-6} emu/mol contribution from the temperature-independent paramagnetic susceptibility in II^{SCO}, a reasonable value for a LS complex at temperatures just below a spin crossover, one finds the presence of either 1.1 wt % of an iron(III) impurity that is assumed to have a moment of 5.92 μ_B or 1.5 wt % of an iron(II) impurity that is assumed to have a moment of 5.20 μ_B. Such a low level of impurity will not be observed in most studies but will be apparent in the magnetic properties of an essentially diamagnetic LS iron(II) complex. Further, as would be expected, both above and below the spin crossover, the inverse molar magnetic susceptibility is linear (see Figure 7a). The rather negative intercept observed for the inverse susceptibility of the HS state is not a consequence of the impurity, but rather is a consequence of a small admixture of the LS state into the predominately HS state above the spin crossover. Such an admixture would also account for the small decrease in the magnetic moment observed between ca. 125 and 225 K.

(29) Long, G. J.; Hutchinson, B. B. *Inorg. Chem.* **1987**, *26*, 608.
(30) (a) Hayami, S.; Gu, Z.-z.; Yoshiki, H.; Fujishima, A.; Sato, O. *J. Am. Chem. Soc.* **2001**, *123*, 11644. (b) Hayami, S.; Gu, Z.-z.; Shiro, M.; Einaga, Y.; Fujishima, A.; Sato, O. *J. Am. Chem. Soc.* **2000**, *122*, 7126. (c) Boèa, R.; Boèa, M.; Dlháò, L.; Falk, K.; Fuess, H.; Haase, W.; Jaroščiak, R.; Papánková, B.; Renz, F.; Vrbová, M.; Werner, R. *Inorg. Chem.* **2001**, *40*, 3025.
(31) Figgis, B. N. *Introduction to Ligand Fields*; Wiley-Interscience: New York, 1966; p 274.
(32) Long, G. J.; Baker, W. A., Jr. *J. Chem. Soc., A* **1971**, 2956.

Table 3. Mössbauer Spectral Hyperfine Parameters for Samples of Fe[(*p*-IC$_6$H$_4$)B(pz)$_3$]$_2$ and Fe[(*p*-IC$_6$H$_4$)B(3-Mepz)$_3$]$_2$ Crystallized under Different Conditions

compound (crystallization conditions)	*T*, K	δ, mm/s[a]	ΔE_Q, mm/s	Γ, mm/s	area, %	assignment
Fe[(*p*-IC$_6$H$_4$)B(pz)$_3$]$_2$	295	0.380	0.32	0.25	100	LS iron(II)
	78	0.447	0.33	0.25	100	LS iron(II)
Fe[(*p*-IC$_6$H$_4$)B(3-Mepz)$_3$]$_2$	295	1.004	3.69	0.23	100	HS iron(II)
(form I^{n}SCO)	78	1.112	3.84	0.26	100	HS iron(II)
Fe[(*p*-IC$_6$H$_4$)B(3-Mepz)$_3$]$_2$	295	1.002	3.68	0.22	100	HS iron(II)
(form II^{SCO})	225	1.045	3.78	0.24	83.5	HS iron(II)
		0.451	0.42	0.27	16.5	LS iron(II)
	155	1.096	3.79	0.26	71.8	HS iron(II)
		0.512	0.42	0.30	28.2	LS iron(II)
	78	1.112	3.82	0.24	9.8	HS iron(II)
		0.542	0.42	0.24	90.2	LS iron(II)
	4.2	0.539	0.43	0.31	100	LS iron(II)
Fe[(*p*-IC$_6$H$_4$)B(3-Mepz)$_3$]$_2$	295	0.999	3.69	0.27	100	HS iron(II)
(form III^{SCO}, dried)	78	1.110	3.83	0.24	21.3	HS iron(II)
		0.538	0.42	0.25	78.7	LS iron(II)
	4.2	1.132	3.80	0.25	21.6	HS iron(II)
		0.543	0.42	0.26	78.4	LS iron(II)

[a] The isomer shifts are given relative to room-temperature α-iron foil.

The effective magnetic moment of the sample that was grown from CH_2Cl_2/MeOH at −20 °C and then air-dried to represent the desolvated form III^{SCO} undergoes a gradual decrease from 4.8 μ_B above 235 K to a constant value of 2.2 μ_B beginning near 140 K (see Figure 7b). The relatively high residual magnetic moment in this sample below 140 K is due predominately to the presence of ca. 20% of I^{nSCO} as an impurity that is clearly observed in the Mössbauer spectra of the samples (see below) and, perhaps to a lesser extent, to the expected temperature-independent paramagnetism of the LS fraction of the desolvated III^{SCO} complex. Once again, as would be expected and may be seen in Figure 7a, the inverse molar magnetic susceptibility is linear both above and below the spin-state crossover.

Mössbauer Spectral Studies. The same samples used for the magnetic studies were subsequently used for Mössbauer spectral studies, and the resulting Mössbauer spectra are shown in Figures 8−10. The spectra have been fit with symmetric quadrupole doublets, and the resulting hyperfine parameters are given in Table 3.

The 295 and 78 K spectra of crushed but unground crystals of Fe[(*p*-IC$_6$H$_4$)B(pz)$_3$]$_2$ indicate that this complex is LS at both temperatures. The observed hyperfine parameters are almost identical to those observed[10,29,33a] for the LS iron(II) in Fe[HB(pz)$_3$]$_2$ at the same temperatures. The only significant difference is an increase in the quadrupole splitting from 0.21 mm/s in Fe[HB(pz)$_3$]$_2$ to 0.32 mm/s in Fe[(*p*-IC$_6$H$_4$)B(pz)$_3$]$_2$, a difference that is reflected in the slightly less distorted coordination environment observed[10a] in the former complex as compared to the latter. By using the structural results[10] of Oliver et al. for Fe[HB(pz)$_3$]$_2$, the average percentage bond distance and bond angle distortion parameters[33b] are found to be 0.24 and 0.18, respectively, whereas the results given in Table 2 for Fe[(*p*-IC$_6$H$_4$)B(pz)$_3$]$_2$ yield the analogous percentage distortions of 0.37 and 0.24, values which are significantly higher.

(33) (a) Grandjean, F.; Long, G. J.; Hutchinson, B. B.; Ohlhausen, L.; Neill, P.; Holcomb, J. D. *Inorg. Chem.* **1989**, *28*, 4406. (b) Renner B.; Lehmann, G. *Z. Krist.* **1986**, *175*, 43.

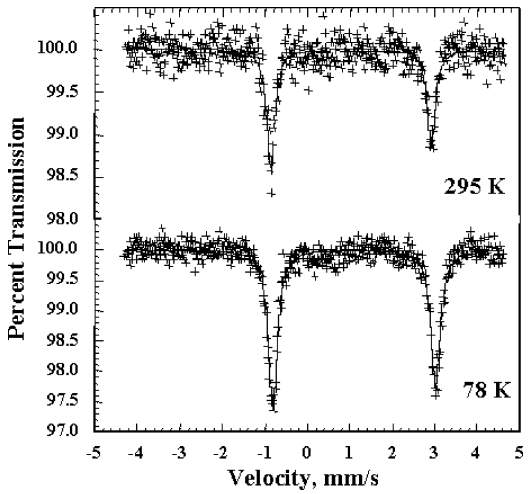

Figure 8. Mössbauer spectra of polymorph I^{nSCO} of Fe[(*p*-IC$_6$H$_4$)B(3-Mepz)$_3$]$_2$ obtained at 295 and 78 K. The solid line corresponds to a fit to the experimental data, +, with the hyperfine parameters given in Table 3.

The 295 K spectrum of crushed but unground crystals of Fe[(*p*-IC$_6$H$_4$)B(3-Mepz)$_3$]$_2$ (I^{nSCO}, Figure 8) indicates that this polymorph is 100% HS with an isomer shift, δ, of 1.004 mm/s and a quadrupole splitting, ΔE_Q, of 3.69 mm/s. These values are similar to the respective 295 K values of 1.06 and 3.8 mm/s observed[26,27] for Fe[HB(3-Mepz)$_3$]$_2$, 1.03 and 3.7 mm/s observed[29] for Fe[HB(3,5-Me$_2$pz)$_3$]$_2$, and 1.04 and 3.7 mm/s observed[29] for Fe[HB(3,4,5-Me$_3$pz)$_3$]$_2$.

The lower isomer shift observed for Fe[(*p*-IC$_6$H$_4$)B(3-Mepz)$_3$]$_2$ as compared with that for Fe[HB(3-Mepz)$_3$]$_2$ indicates a somewhat higher s-electron density at the iron-57 nucleus in the former complex. It would be tempting to associate this increased s-electron density with electron donation by the *p*-IC$_6$H$_4$ substituent on the ligand, but this substituent is surely too remote to have a significant influence on the s-electron density at the iron(II) ion. Thus, it seems more likely that the higher s-electron density is a consequence of the shorter average Fe−N bond distance of 2.18 Å observed in Fe[(*p*-IC$_6$H$_4$)B(3-Mepz)$_3$]$_2$ as compared with the distance of 2.20 Å observed[26] in Fe[HB(3-Mepz)$_3$]. Further, the slightly smaller quadrupole splitting observed

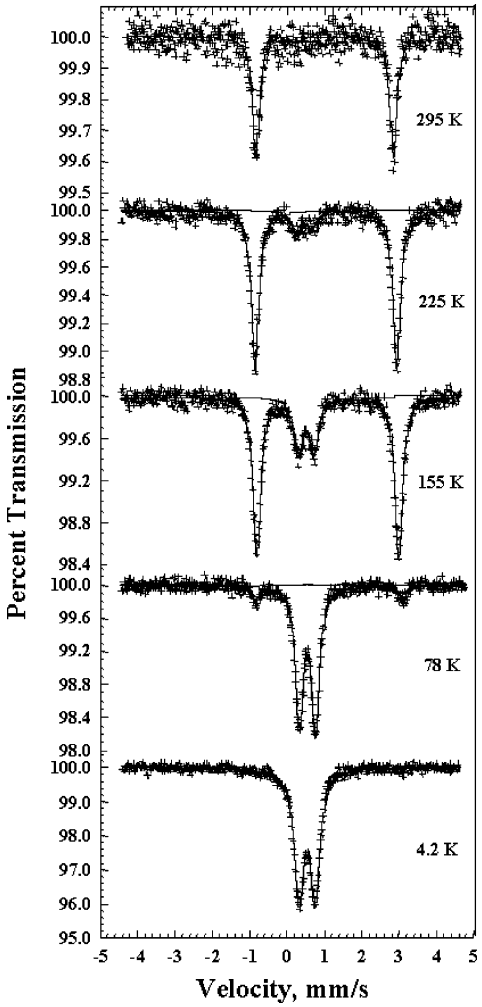

Figure 9. Mössbauer spectra of polymorph II^{SCO} of Fe[(*p*-IC$_6$H$_4$)B(3-Mepz)$_3$]$_2$ obtained at several temperatures between 295 and 4.2 K. The solid line corresponds to a fit to the experimental data, +, with the hyperfine parameters given in Table 3.

in Fe[(*p*-IC$_6$H$_4$)B(3-Mepz)$_3$]$_2$ as compared with that observed[26,27] in Fe[HB(3-Mepz)$_3$]$_2$ is probably a consequence of the smaller distortions observed in the former complex (see above).

Upon cooling of the sample to 78 K, the isomer shift of the I^{nSCO} form of Fe[(*p*-IC$_6$H$_4$)B(3-Mepz)$_3$]$_2$ increases to 1.112 mm/s as a result of the second-order Doppler shift, but no other spectral changes are observed, and I^{nSCO} remains completely HS, as would be expected from its observed magnetic moment at low temperature.

The Mössbauer spectra of an absorber containing crushed but unground crystals of the II^{SCO} polymorph of Fe[(*p*-IC$_6$H$_4$)B(3-Mepz)$_3$]$_2$ are shown in Figure 9. As expected from the observed magnetic moment (see Figure 7), the 295 K spectrum of II^{SCO} shows a single HS iron(II) quadrupole doublet with an isomer shift of 1.002 mm/s and a quadrupole splitting of 3.68 mm/s, parameters which are virtually identical to those of I^{nSCO}. However, upon cooling of the sample, the behavior of II^{SCO} is very different from that of I^{nSCO}, as may be seen by a comparison of Figures 8 and 9. Upon cooling, a second quadrupole doublet corresponding to LS iron(II) appears with a relative area of 16.5% at 225 K. The relative area of this doublet increases to 28.2% at 155 K, predominates with a relative area of 90.2% at 78 K, and is the only component observed at 4.2 K; the resulting 4.2 K isomer shift of 0.539 mm/s and quadrupole splitting of 0.43 mm/s are typical of a LS iron(II) complex. This behavior is completely consistent with an iron(II) complex undergoing a complete HS-to-LS state crossover and agrees with the magnetic properties shown in Figure 7.

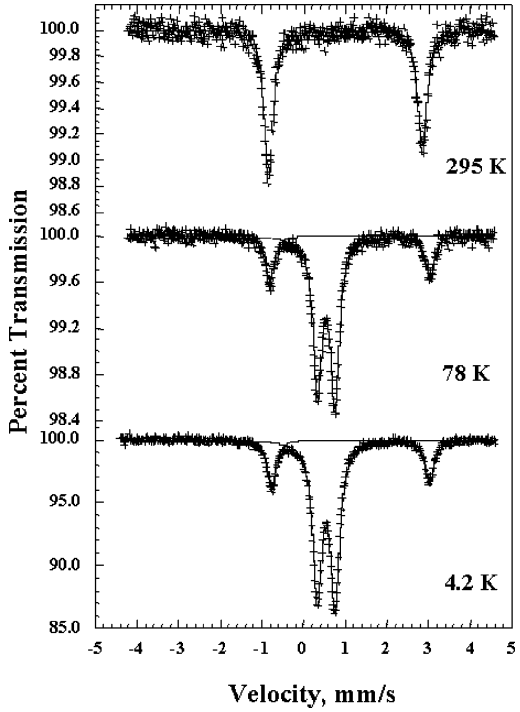

Figure 10. Mössbauer spectra of the desolvated form of III^{SCO}, Fe[(*p*-IC$_6$H$_4$)B(3-Mepz)$_3$]$_2$, obtained at 295, 78, and 4.2 K. The solid line corresponds to a fit to the experimental data, +, with the hyperfine parameters given in Table 3.

The variable-temperature Mössbauer spectra (see Figure 10) of the sample obtained at −20 °C from MeOH/CH$_2$Cl$_2$ and then air-dried and containing predominately desolvated crystals of III^{SCO} are very similar to the spectra observed for I^{nSCO} and II^{SCO}. Thus, the 295 K spectrum is fully HS, but at both 78 and 4.2 K, the spectra exhibit the presence of ca. 80% by area of a LS quadrupole doublet that may be associated with III^{SCO} and 20% by area of a HS quadrupole doublet that may be associated with the impurity of I^{nSCO}.

It is worth noting that the LS iron(II) isomer shift of 0.54 mm/s observed at 78 K for both II^{SCO} and III^{SCO} is significantly larger that the 0.47 mm/s value observed[29] in Fe[HB(pz)$_3$]$_2$. Further, the LS quadrupole splitting of 0.42 mm/s observed at 78 K for both II^{SCO} and III^{SCO} is significantly larger that the 0.22 mm/s splitting observed[29] in Fe[HB(pz)$_3$]$_2$ and the 0.33 mm/s splitting observed in Fe[(*p*-IC$_6$H$_4$)B(pz)$_3$]$_2$. All of these differences are those expected from a comparison of the average bond distances and the average percentage bond distortion parameters[33b] observed for Fe[HB(pz)$_3$]$_2$, Fe[(*p*-IC$_6$H$_4$)B(pz)$_3$]$_2$, and both II^{SCO} and III^{SCO}. In all cases, the percentage distortion parameters for II^{SCO} and III^{SCO} are larger than for the other two complexes.

Discussion

The Fe[(*p*-IC$_6$H$_4$)B(pz)$_3$]$_2$ complex, like the related Fe[PhB(pz)$_3$]$_2$ complex, is LS at room temperature. In contrast, the 3-methyl-substituted Fe[(*p*-IC$_6$H$_4$)B(3-Mepz)$_3$]$_2$ complex is HS at room temperature as a consequence of the added steric interactions involving the six added 3-methyl substituents.

Initially, the spin-state crossover exhibited by Fe[(*p*-IC$_6$H$_4$)B(3-Mepz)$_3$]$_2$ appeared to be sample dependent, but it was later found to be a consequence of the changing relative distributions of the two polymorphs, I^{nSCO} and II^{SCO}, and/or the (desolvated) solvate, III^{SCO}, in the samples. Once conditions were found that produced each polymorph in relatively high purity, it was found that the polymorphs exhibited remarkably different electronic properties as a result of differences in their crystal packing. Form I^{nSCO} crystallizes with a highly ordered three-dimensional supramolecular structure and does not undergo a spin-state crossover upon cooling. In contrast, form II^{SCO}, with a stacked two-dimensional supramolecular structure, undergoes a reversible and abrupt spin-state crossover between 126 and 131 K.

Qualitatively, the temperature dependence of the spin-state crossover in single crystals of the third form, III^{SCO}, is different from that of the second form, as can be seen by the gradual crystal color changes in Figure 3 over similar temperature ranges. Quantitative magnetic or Mössbauer measurements on the solvated form were not possible due to the rapid loss of the solvent. Bulk samples of the third form were grown at −20 °C and were air-dried to completely remove the solvent in the lattice. The magnetic data obtained on these desolvated crystals showed a gradual transition between about 140 and 235 K from the HS to the LS state, as is confirmed by the Mössbauer spectra. The structure of desolvated form III^{SCO} is unknown but is likely only a weakly associated structure, at best, given that even the crystalline form of the solvate is a loosely packed two-dimensional structure organized by only weak CH−π interaction.

An examination of the temperature dependence of the effective magnetic moment of the three forms reveals several features. First, form I^{nSCO} does not undergo any electronic spin-state crossover at temperatures above 4 K; second, form II^{SCO} exhibits an abrupt crossover between 126 and 131 K; and, third, the desolvated form III shows a gradual transition between 140 and 235 K. The solid-state structure of each of the first two polymorphs is organized by several noncovalent interactions, whereas it is likely that the desolvated third form is not highly organized. The abrupt nature of the spin-state crossover in II^{SCO} can be envisioned to result from the geometry changes associated with the spin-state crossover, changes that are propagated throughout the crystal via the noncovalent interactions that occur in the *bc*-plane of the crystal.

The relative robustness of the sheet structure is also manifested in changes in the crystal geometry upon cooling (see Figure 11). For II^{SCO} there is a 6% decrease in unit cell volume, from 1998 Å^3 at 294 K to 1877 Å^3 at 100 K. Of the axes involved in the change, the *a*-axis, along which the noncovalent sheets structures are loosely stacked, exhibits the largest change, an ca. 5.2% compression from 11.05 Å at 294 K to 10.47 Å at 100 K. In comparison, the changes in the other two axes, where the noncovalent network is strong, are much less dramatic. Indeed, the *b*-axis, which contains the CH(pz)−π(pz) interactions, actually *expands* by 0.6% on cooling, from 15.71 Å at 294 K to 15.80 Å at 100 K, whereas the *c*-axis, which contains the CH(arene)−π-(pz) interactions, contracts by only ca. 2.1% on cooling, from 11.81 Å at 294 K to 11.56 Å at 100 K. These large, directionally oriented changes are contrasted by the changes observed for I^{nSCO,} where the dimensions in all three directions slowly contract linearly as the temperature is lowered, the result expected for this compound with a three-dimensional supramolecular structure that exhibits no spin crossover.

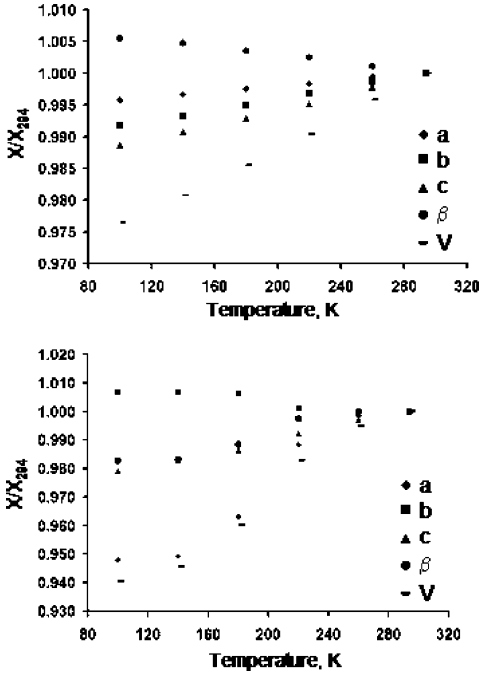

Figure 11. Temperature dependence of the relative cell parameters, a/a_{294}, b/b_{294}, c/c_{294}, and β/β_{294}, and the cell volume in the I^{nSCO} (top) and II^{SCO} (bottom) polymorphs of Fe[(*p*-IC$_6$H$_4$)B(3-Mepz)$_3$]$_2$.

The observation that form II^{SCO}, with the less organized structure, undergoes a crossover from the HS to the LS state, whereas no such change is observed in I^{nSCO}, is in agreement with the general observations by others[30] that the "spin-state crossover phenomenon depends strongly on intermolecular interactions."[30b] The unique result reported herein is that the comparison is made with polymorphs in which comparisons of the supramolecular structures can be made on two different crystalline polymorphs of the same *molecular* compound. It is clear from these results that the organization of the molecules in the solid state controlled by the noncovalent interactions has a significant impact on the spin-crossover temperature; the more highly organized structure better resists the crossover to the LS state at low temperature. The third form, the desolvated form of III^{SCO}, also supports this trend in that the solid-state form used in the magnetic and Mössbauer studies certainly has a less organized structure

than the other two forms and it has the highest $T_{1/2}$. In addition, as revealed by the magnetic results shown in Figure 7, II^{SCO} exhibits a much more "cooperative" spin-state crossover changeover than does III^{SCO}, as would be expected because of its more highly organized solid-state structure.

These results are consistent with previous observations that the driving force for the spin-state crossover from LS to HS iron(II) is dominated by the entropy term associated with the electronic reorganization and the associated bond expansion and ligand deformation processes. One can envision that the HS state of form I^{nSCO} is energetically "locked-in" by the multiple noncovalent interactions that prevent the spin-state crossover from occurring; the net result would be a stabilization of the HS state. Calorimetry measurements have provided transition enthalpies, ΔH, of 6−15 kJ/mol and entropies, ΔS, of 40−50 J/Kmol for charge-neutral iron(II) spin-state crossover complexes.[1] If the polymorphs of Fe[(*p*-IC_6H_4)B(3-Mepz)$_3$]$_2$ fall into the middle of these ranges, i.e., $\Delta H = 10$ kJ/mol and $\Delta S = 45$ J/Kmol, and if the crossover temperature of I^{nSCO} is at least 130 K lower than that of II^{SCO}, then the energy difference in the spin crossover of II^{SCO} and a hypothetical transition for I^{nSCO} are more favorable in the former polymorph by about 6 kJ/mol. This value appears to correlate well with the proposed interaction energy[25,28] (0.5−15 kJ/mol) and number of weak noncovalent interactions stabilizing the crystals of I^{nSCO} and II^{SCO}, where more interactions are observed in the three-dimensional structure of I^{nSCO}. Likewise, the energy difference in the spin transitions between II^{SCO}, with a $T_{1/2}$ of 128 K, and the disorganized, and possibly amorphous, desolvated III^{SCO}, with a $T_{1/2}$ of 175 K, is of the order of 2 kJ/mol.

Conclusions

The spin-state crossover behavior of poly(pyrazolyl)borate iron(II) compounds can be dramatically affected by their supramolecular structures, as is shown herein through a comparison of solid-state structures and magnetic and Mössbauer spectral studies of the polymorphs of Fe[(*p*-IC_6H_4)B(3-Mepz)$_3$]$_2$. Noncovalent interactions, such as $\pi-\pi$, CH$-\pi$, and other weak hydrogen-bonding interactions, such as CH−halide interactions, provide a vehicle for controlling the geometric changes and can result in abrupt spin-state crossover temperature ranges and even prevent the changeover from occurring at low temperatures. From the current study, we find that, for a given donor set, the more highly organized structures will have lower spin-crossover temperatures and more abrupt spin crossovers than those with less highly or more "loosely" organized structures.

Acknowledgment. We thank Dr. Matthew J. Davis and William Gemmill for assistance with the measurements made with the SQUID magnetometer. We acknowledge with thanks the National Science Foundation (CHE-0414239) and the Petroleum Research Fund (36368-AC3) for support. The Bruker CCD single-crystal diffractometer was purchased using funds provided by the NSF Instrumentation for Materials Research Program through Grant DMR:9975623. L.R. and F.G. acknowledge with thanks the financial support of the Fonds National de la Recherche Scientifique, Belgium, through grants 9.456595 and the Ministère de la Région Wallonne for grant RW/115012.

Supporting Information Available: CIF files for Fe[(*p*-IC_6H_4)B(3-Rpz)$_3$]$_2$ (R = H and R = Me, three forms at various temperatures). This material is available free of charge via the Internet at http://pubs.acs.org.

IC048406Q